RADIATIVE PROTON CAPTURE BY ^{63}Cu

by

Kuen-hwang Huang

Submitted to the Faculty of Graduate Studies

In Partial Fulfillment of the Requirements

For the Degree of Master of Science

Department of Physics
Faculty of Science and Engineering
University of Ottawa
Ottawa, Canada

ABSTRACT

A target about 3 Kev thick of ^{63}Cu was bombarded with protons of energy from 1.32 Mev to 2.18 Mev. One hundred and sixteen resonances were observed in the ^{64}Zn compound nucleus. The level density of ^{64}Zn was plotted and compared with three theoretical calculations. The six energy levels of ^{64}Zn, 9.400, 9.554, 9.598, 9.672, 9.736 and 9.753 Mev appear to be the analogue states of the ground state, 0.159, 0.205, 0.278, 0.344, and 0.362 Mev of ^{64}Cu respectively. If so, the coulomb energy difference of $^{64}Zn \sim {}^{64}Cu$ should be 9.605 ± 0.005 Mev according to the present work. Gamma-ray measurements of three strong resonances have been performed with a Ge(Li) detector and the decay schemes have been constructed. The experimental Q-value of $^{63}Cu(p, \gamma)^{64}Zn$ was determined to be 7.708 ± 0.003 Mev.

ACKNOWLEDGEMENTS

I would like to thank my supervisor, Dr. B. Hird, for his interest in this work, for his useful suggestions about this thesis and for some financial support.

I wish to extend a very special thanks to Dr. H. L. Pai and Dr. T. H. Hsu for their help, their interest and most useful discussions.

Appreciation is also extended to Dr. A. L. Carter for making the stabilized spectrometer system from which the excellent energy calibration of γ-ray and data analysis were obtained. And Dr. R. L. Clarke for his suggestion about Nuclear Level density for this thesis.

I would like also to thank all those persons involved with the operation and maintenance of the Dynamitron Accelerator for their co-operation.

TABLE OF CONTENTS

TABLES

FIGURES

page

CHAPTER I INTRODUCTION

The γ rays from proton bombardment of copper were first measured by Malich and Harris[1]. No sharp resonances were observed by them except that the thick target yield increased nearly exponentially, and the yield was comparable to that from a thick aluminum target. Later, several low energy levels were found by Weller and Grosskreutz[2], but no measurements have been reported for the reaction $^{63}Cu(p, \gamma)^{64}Zn$ at an excitation energy greater than 9 Mev.

The present work consists of measurements of the reaction $^{63}Cu(p, \gamma)^{64}Zn$ using a proton energy from 1.32 Mev to 2.18 Mev which corresponds to an excitation energy from 9 Mev to 9.85 Mev. The level density of ^{64}Zn was plotted and compared with three theoretical calculations; Bethe's theory, the method of Newton and Cameron, and the method of Gilbert and Cameron. Some strong resonances are thought to be the analogue states of ^{64}Cu. Gamma-ray measurements of three strong resonances were performed with a Ge(Li) detector. The data were used to construct the Level scheme of ^{64}Zn.

CHAPTER II GENERAL PROCEDURE

The 3 Mev Dynamitron Accelerator was used as a source of protons. This accelerator provides up to 50 microamperes of protons over the energy range from 0.5 Mev to 2.5 Mev, with an energy spread of about 0.1%.

The measurements conducted in the present study were as follows: (a) the excitation curves for $^{63}Cu(p, \gamma)^{64}Zn$ reaction over the energy range E_p = 1.3 Mev to 2.18 Mev, (b) the decay scheme of the three strong resonances, E_p = 1922 Kev, 2056 Kev and 2094 Kev.

(A) Detecting Equipment

(a) The electronics for the NaI(Tl) detector system.

In order to obtain excitation curves, a 3 in x 3 in NaI(Tl) crystal was placed at 90^o to the beam and at about 2 cm from the target. The block diagram of the electronics which were used in this experiment is shown in Figure 1. Signals from the gamma-ray detector were preamplified[(a)] and then amplified by a shaping amplifier[(b)]. The logic pulses were obtained from the

(a) ORTEC Model 113 Scintillation preamplifier
(b) ORTEC Model 410 Multimade Amplifier

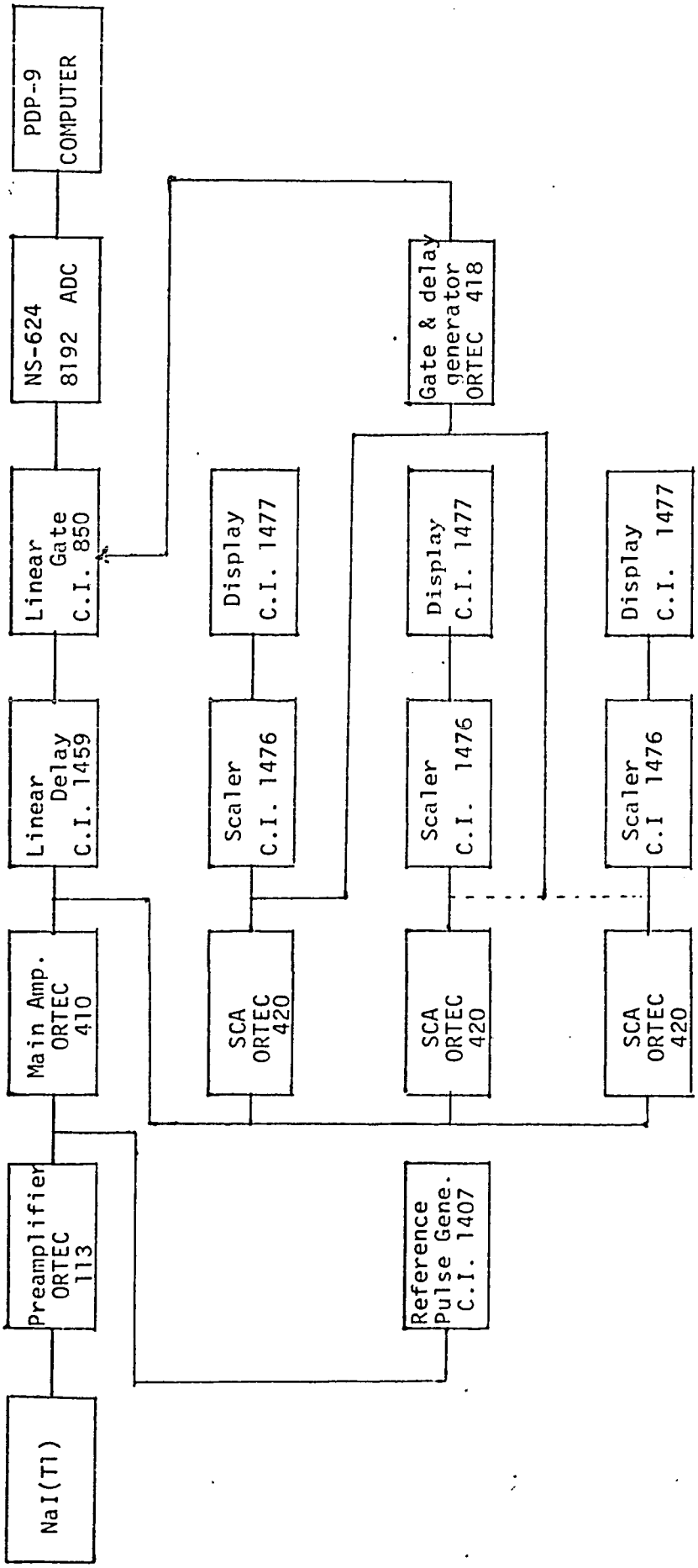

Figure 1: The block diagram of the electronics for $Cu^{63}(p, \gamma)Zn^{64}$ excitation curve.

signals by means of a single channel analyser[c]. They were fed through a gate and delay generator[d] and then to gate[e] the analog-pulse which came from the signal amplifier by way of linear delay[f]. Then the output pulse of the linear delay went into the analog-to-digital converter (ADC)[g] which was interfaced on-line with a PDP-9 computer.

The pulse generator[h] was used to normalise the pulse height of the standard sources for calibration and for setting the window of the three SCA, which separately connected with the scaler[i] and the display[j] for measurement of the counting rate for this experiment.

(b) The electronics for the Ge(Li) detector system

The 26 cc Ge(Li) detector was placed on the opposite side of the target to the NaI(Tl) detector at a distance of about 2 cm from the target. The electronics are shown in Figure 2.

(c) ORTEC Model 420 Single Channel Analyser
(d) ORTEC Model 418 Gate and Delay Generator
(e) C. I. Model 850 Linear Gate
(f) C. I. Model 1459 Linear Delay
(g) NS-624 8192 Analog-to-Digital Converter (ADC)
(h) C. I. Model 1407 reference pulse generator
(i) C. I. Model 1476 Scaler
(j) C. I. Model 1477 Display

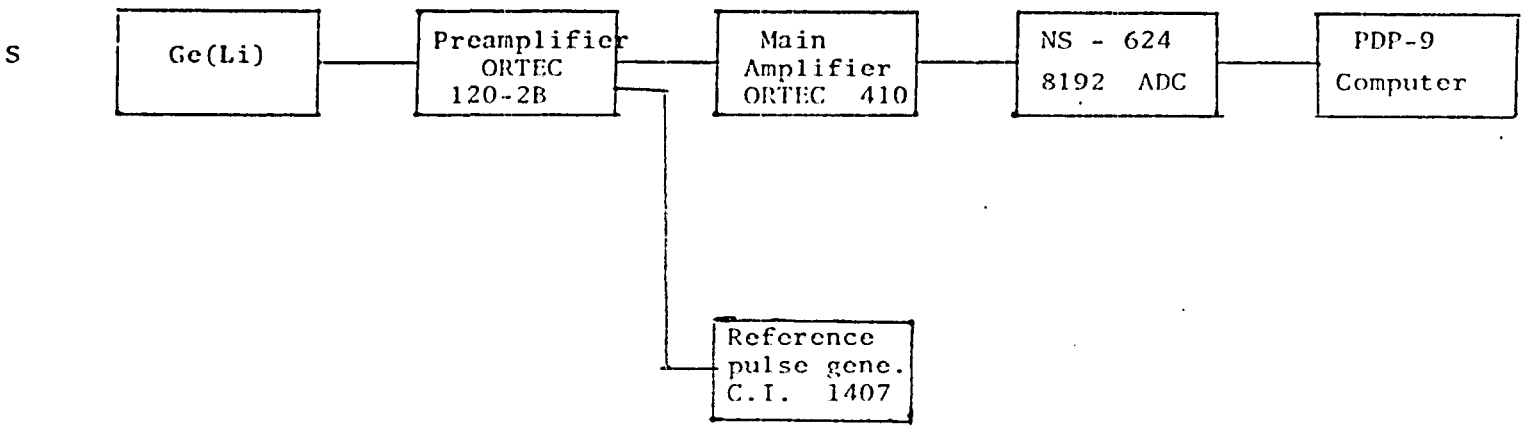

Figure 2. The block diagram of the electronics for Ge(Li) detector system.

(B) Target Preparation

The enriched copper metal (99.99% ^{63}Cu) was evaporated onto a gold backing which was 0.25 mm thick. Great care was taken in making the target. The boat which was used to make the target must first be heated in vacuum by increasing the current to about 200 amperes in order to evaporate the contaminants which exist on the surface. Then the sample was placed in the boat and the distance between the sample and the evaporated gold plate was adjusted, depending on the thickness required. By increasing the current slowly to 150 amperes during two minutes the clean target of the copper and aluminum were made. The thickness of the target depends on the quantity of the sample and the distance between the gold plate and the sample. Several different thicknesses of targets were made for this experiment. The best target was found to be about 3 Kev in FWHM on resonance measurements. For this thickness a sample of 4 mg and a distance of 8 cm were used.

(C) Target Protection and Target Chamber Design

Even these "clean" targets did not remain uncontaminated long once they were placed inside the Dynamitron vacuum system and bombarded. A rather rapid buildup of fluorine and carbon were

observed on a fresh copper target during the first hour of bombardment. It is very important to keep the target free from those unexpected sources. But it is very difficult to do it. Several target chamber configurations were evaluated. The best design was found to be that shown in Figure 3. The targets were surrounded at liquid-nitrogen temperature by the cold trap[k]. The target support [L] could be moved up and down and rotated to expose either side. Two targets were set on the front side and two on the rear side. The whole target chamber became a Faraday cup which allowed precise measurements of beam current.

In addition to providing protection against fluorine and carbon contamination, this target chamber effectively prevented any other type of contamination, such as the formation of oil films over the target, with subsequent molecular cracking by the beam. Targets which had been bombarded with 10 microamperes of protons for 24 hours showed no visible traces of carbon. A film of carbon would cause the attenuation of the energy of the incident proton beam producing bad energy resolution of the peak of the resonance. Such a condition would not permit the separation

(k) The cold trap was used by Dr. H. L. Pai before
(L) Target support was designed by Dr. T. H. Hsu.

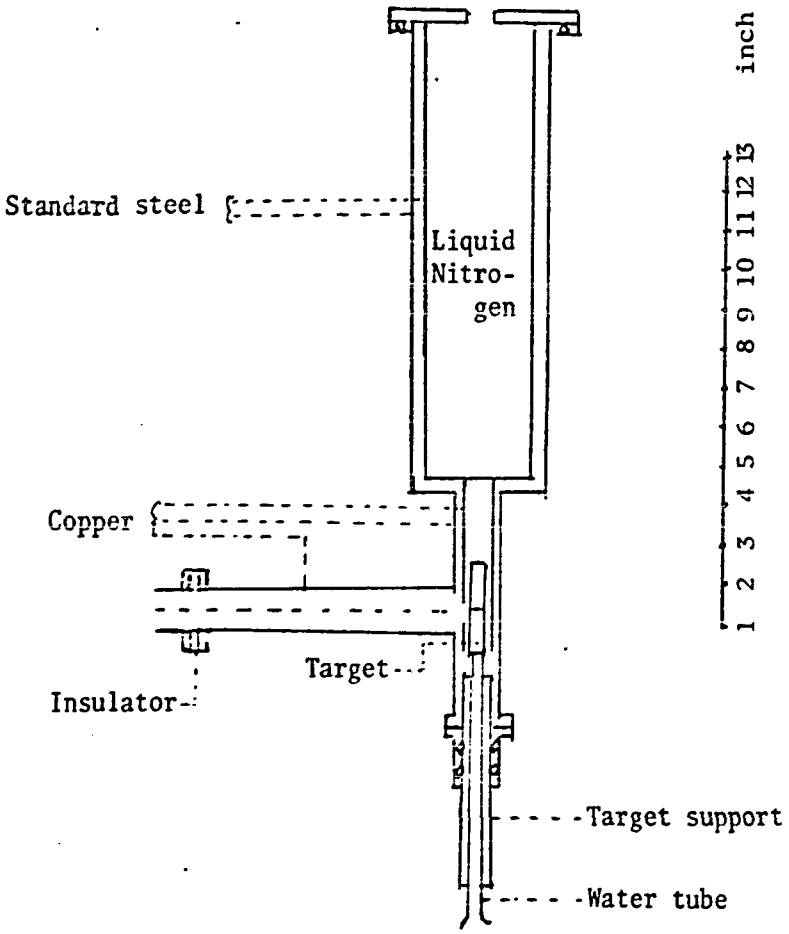

Figure 3: Target chamber and Target support.

of close resonances. This target chamber also produced better yields for this experiment.

(D) Energy Calibration

Two energy calibrations were required for this experiment: (a) the proton energy calibration and (b) the gamma-ray energy calibration. It was very important to maintain the temperature of the electronics constant in order to guard against any gain or zero level drift in the electronic system while the spectra were being taken. The stability was achieved by using the standard source before the calibrations were performed.

(a) The proton energy calibration

The known energies of $^{27}Al(p, \gamma)^{28}Si$ resonances[17, 18] were used to calibrate the unknown energy of $^{63}Cu(p, \gamma)^{64}Zn$ resonances. Since shifts of 5 - 10 Kev in the beam energy could be expected in the course of a day, or after machine sparking, a great deal of care was taken in determining as accurately as possible the energy of resonances. The calibration was done for the energy interval around 50 Kev. These known E_p with their corresponding reading of the digital volt meter (DVM) were fitted by computer using the method of least squares. The

linear relationship between E_p and DVM was shown in Figure 4.

(b) Gamma-ray energy calibration *

The gamma-ray spectra taken by Ge(Li) detector were calibrated by the following well-known energies: (1) 898 Kev and 1836.13 Kev from standard source ^{88}Y, (2) 1274.55 Kev from standard source Na^{22}, (3) 2614.47 Kev from standard source Th, (4) 1368.53 Kev from $^{23}Na(n,\gamma)\ ^{24}Na$ reaction, (5) 6129.3 Kev, 5618.29 Kev, and 5107.29 Kev from the full-energy, single escape and double-escape of $^{19}F(p, \alpha\gamma)O^{16}$. These energies with their corresponding channel number were fitted by linear least squares. Analysis showed a linear relationship between energy and channel number from 0.5 Mev to 11 Mev. The maximum deviation from linearity was 1.2 Kev.

The resonance energy which was measured by the NaI(Tl) detector with the method of the proton energy calibration was in excellent agreement with the energy of the ground state transition as measured by the method of the gamma-ray energy calibration. The difference between them was less than 3 Kev.

* See Figure 16 in appendix

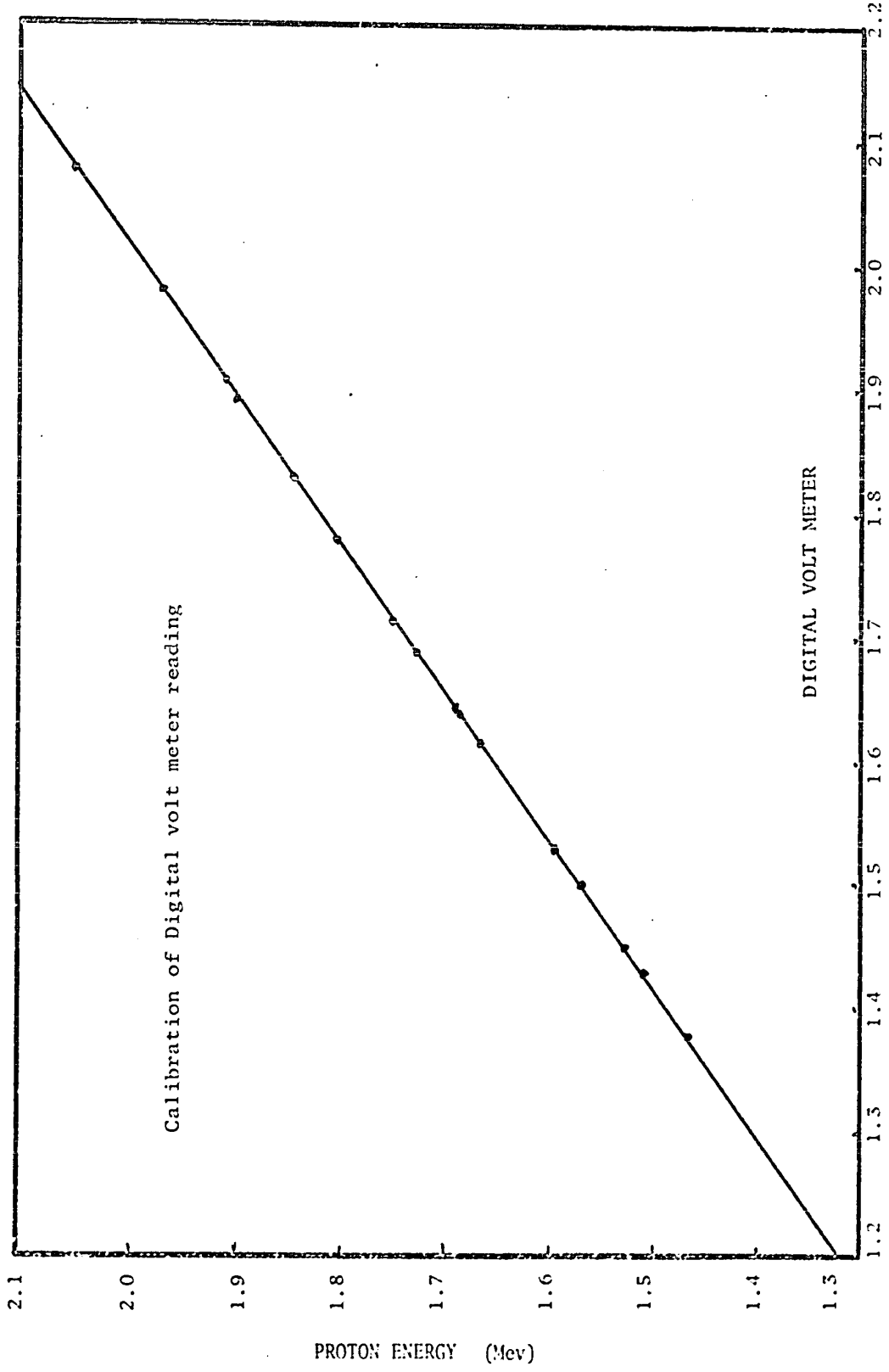

Figure 4. The Calibration of the Digital meter reading by ^{27}Al (p, γ) ^{28}Si reaction.

CHAPTER III EXCITATION CURVE

The excitation curve was first taken in 2 Kev steps with a target about 10 Kev thick from 1.3 Mev to 2.2 Mev incident proton energy with the three gates set at 0.99 Mev to 1.01 Mev, 5 Mev to 10 Mev and 8.5 Mev to 10 Mev respectively (results not shown). The first gate had the highest counting rate and the most background. The counting rate of the second was not good enough for statistics at low energy. The third gate was set to count exclusively the resonance to the ground state transition.

The thick target did not allow sufficient resolution for the high density of states encountered. For this reason, a target of 3 Kev thickness was substituted for final measurements of the excitation curve. These measurements were taken in 2 Kev steps from 1.3 Mev to 1.64 Mev and in 1 Kev steps from 1.64 Mev to 2.18 Mev. Each step was a charge of 8×10^2 micro-coulombs. The excitation curves with gate 0.99 Mev to 1.01 Mev for Ep = 1.3 Mev - 2.18 Mev were shown in Figure 5-1, 5-2 and 5-3. *

* The excitation curves with statistics error were shown in Figure 17-1, 17-2, 17-3, 17-4, 17-5, 17-6 and 17-7 in Appendix.

The general background was taken using the first gate with a gold plate target. Some strong resonance peaks with background could be seen in Figure 6, in which curve-A was general background, the small peak c in 1748 Kev on curve-A was from the $^{13}C(p,\gamma)^{14}N$ reaction and a broad small peak F was from the $^{19}F(p,\alpha\gamma)^{16}O$ reaction. It appeared that the general background was very low compared with the valleys of the peaks. The beam energy spread and the thickness of the target caused these high valleys.

The Ge(Li) detector was used to examine the $^{63}Cu(p,p'\gamma)^{63}Cu$ and $^{63}Cu(p,\alpha\gamma)^{60}Ni$ reactions during the measurement of the excitation curve with the 0.99 Mev gate. The 0.669 Mev gamma-ray produced by a transition from the first excited state to the ground state in ^{63}Cu appeared very strong, but not the 0.962 Mev of the gamma-ray which corresponded to the energy of transition from the second excited state to the ground state in ^{63}Cu. The 1.3325 Mev peak which corresponded to the energy from the first excited state to the ground state in ^{60}Ni did not appear in the Ge(Li) detector spectra either. This might be due to the low probability of the quantum mechanical tunneling of the alpha particle though the high coulomb barrier in the compound nucleus

^{64}Zn, since the Q-value of $^{63}Cu(p,\alpha\gamma)^{60}Ni$ reaction is only 3.7518 Mev. The 6.1293 Mev 5.61829 Mev and 5.10729 Mev peaks from the full-energy, single-escape and double-escape of $^{19}F(p,\alpha\gamma)^{16}O$ came with every resonance of $^{63}Cu(p,\gamma)^{69}Zn$. These were more valuable for energy calibration.

Numerical values of the resonance energies and the corresponding excitations were listed in table 1-1, 1-2 and 1-3. The Q-value of 7.7062 Mev was calculated according to the reference (19) 116 resonances have been assigned to the reaction $^{63}Cu(p,\gamma)^{64}Zn$ in the energy region 1.3 Mev - 2.18 Mev. The width of the resonance peak not only depends on the energy spread of the incident proton beam which was about 2 Kev at 2 Mev proton energy, but also depends on the thickness of the target. The Doppler broadening was reduced by orienting the detector at an angle of 90^{o} to the direction of the incident proton beam. As each resonance did not stand out as an isolated peak, it was quite obvious that not all resonances in this energy region were resolved.

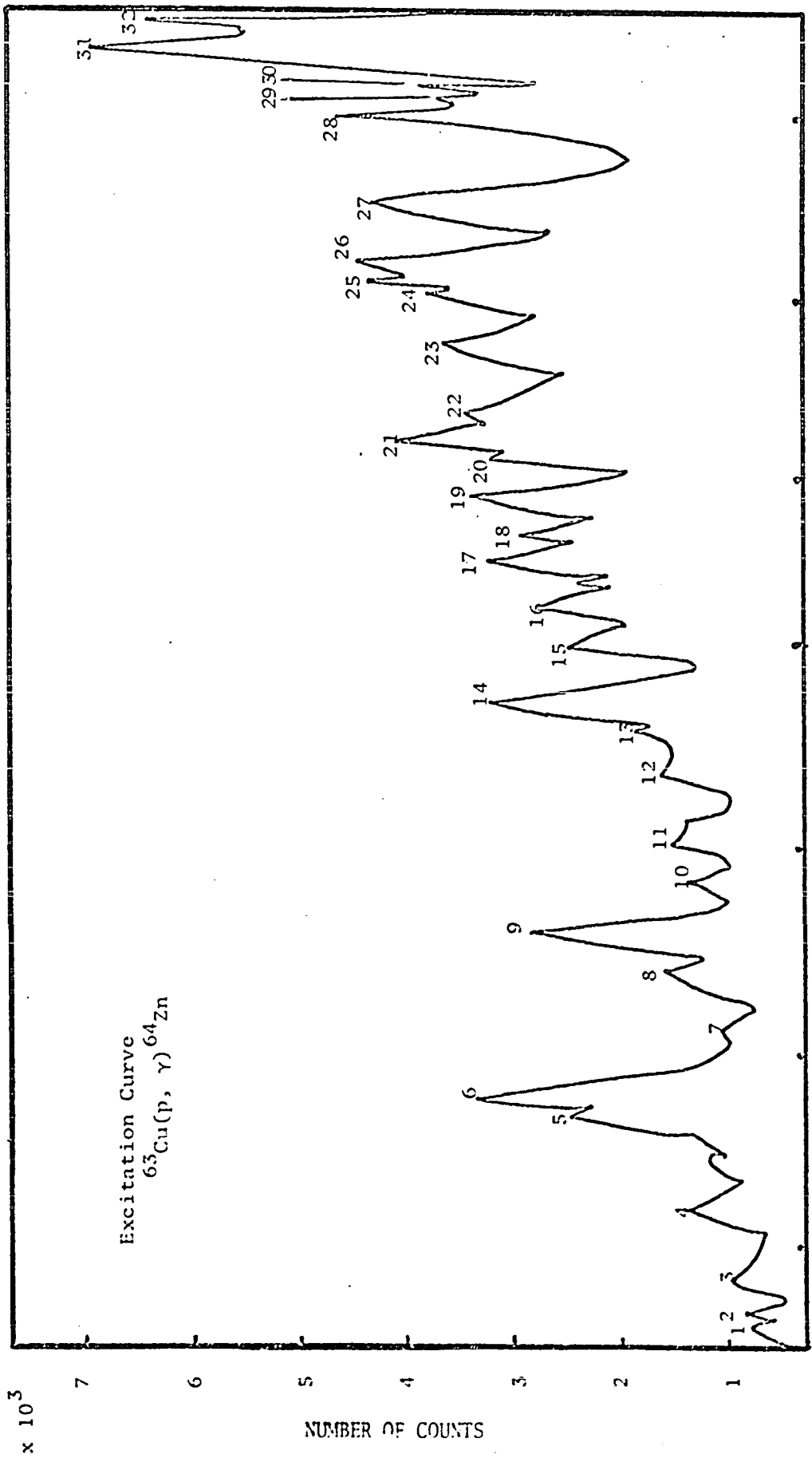

Figure 5-1: Excitation curves from $Cu^{63}(p, \gamma)Zn^{64}$ reaction with gate 0.99 Mev.

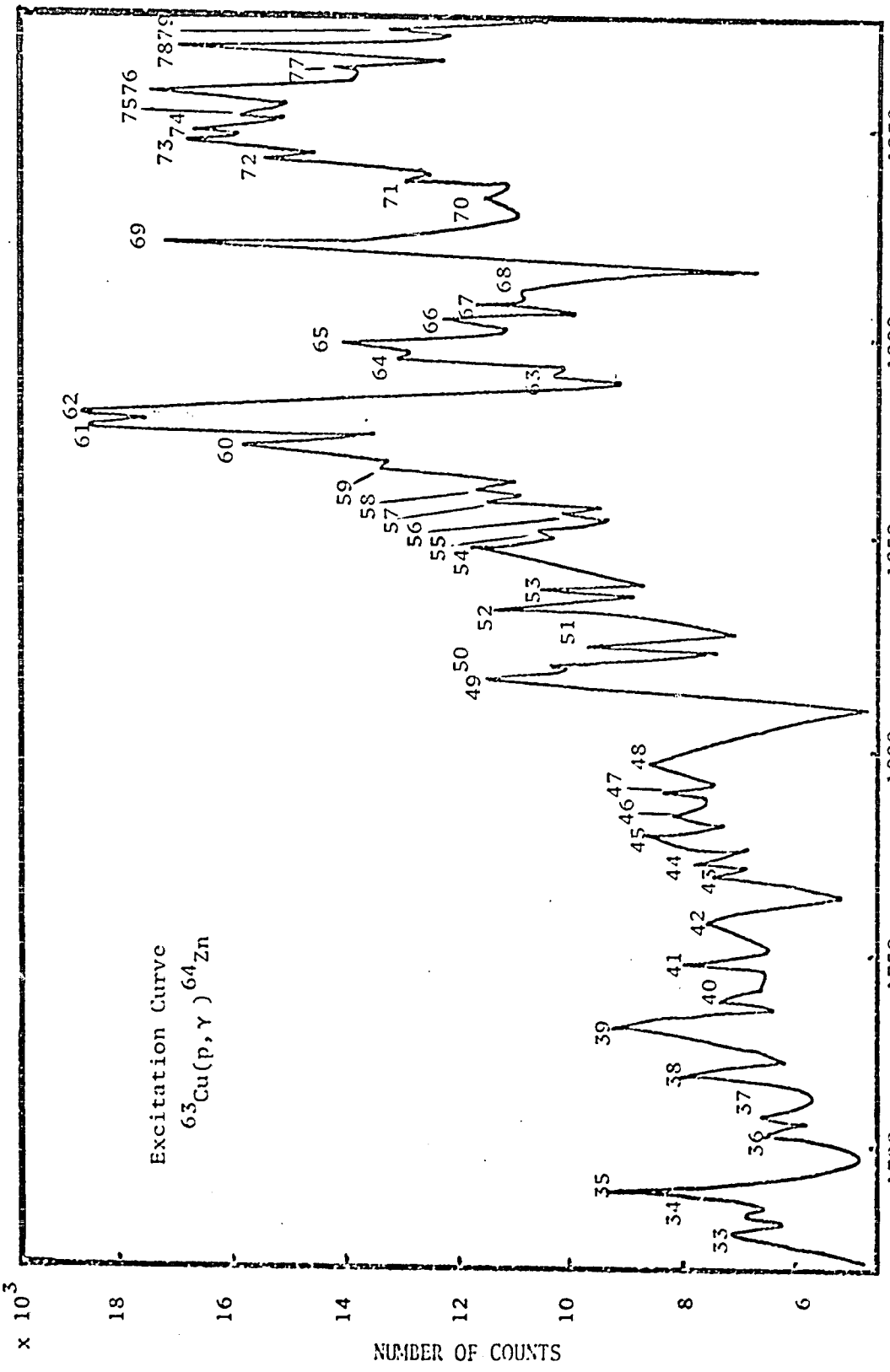

Figure 5-2: Excitation curves from $Cu^{63}(p, \gamma)Zn^{64}$ reaction with gate 0.99 Mev.

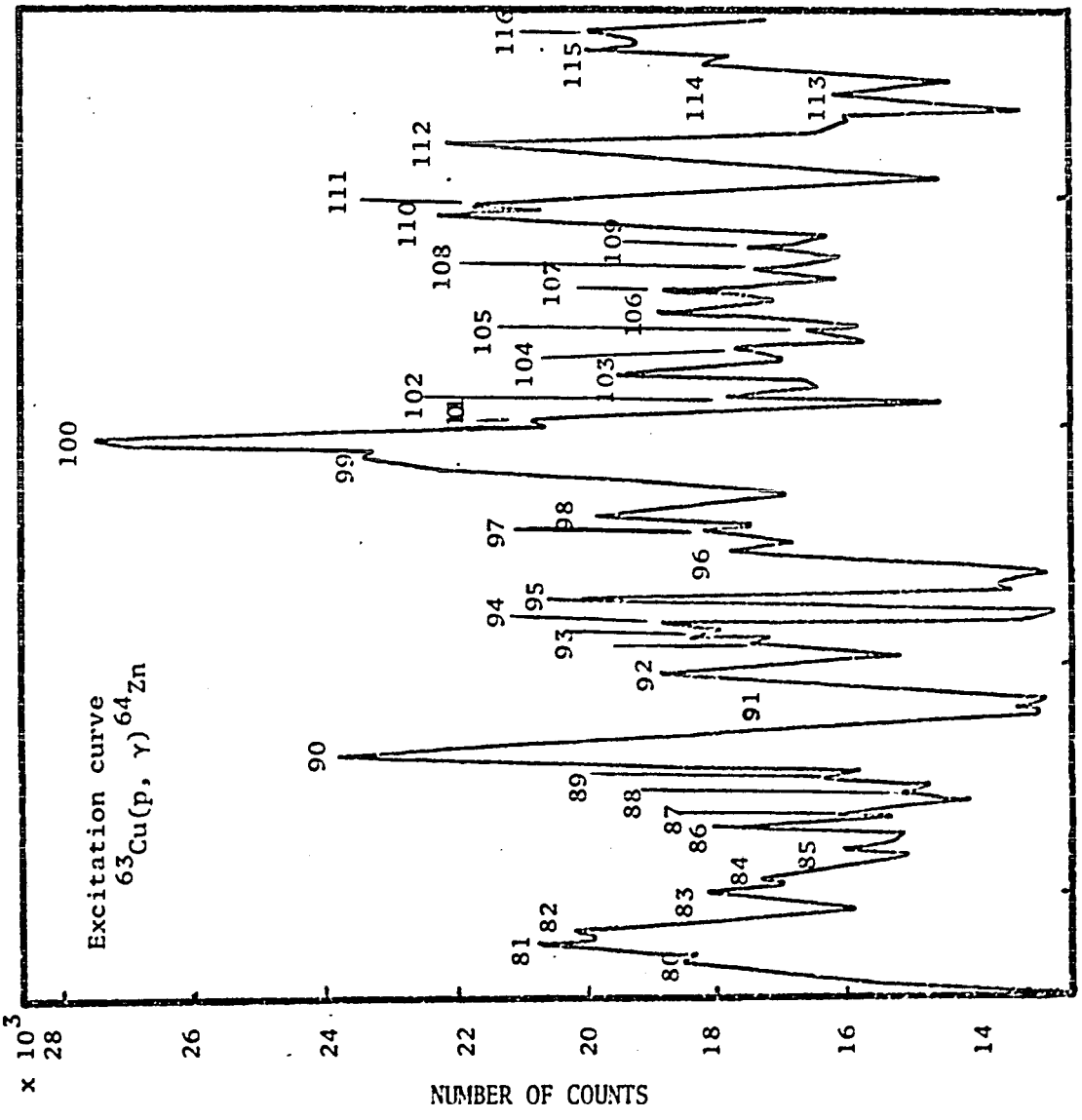

Figure 5-3: Excitation curves from $Cu^{63}(p, \gamma)Zn^{64}$ reaction with gate 0.99 Mev.

Figure 6 Some strong resonances in $Cu^{63}(p, \gamma)^{64}Zn$ were compared with general background. Curve A is general background, F is $^{19}F(\alpha,\alpha\gamma)^{16}O$ reaction in 1375 Kev; C is the peak of $^{13}C(p, \gamma)^{14}N$ reaction in 1448 Kev.

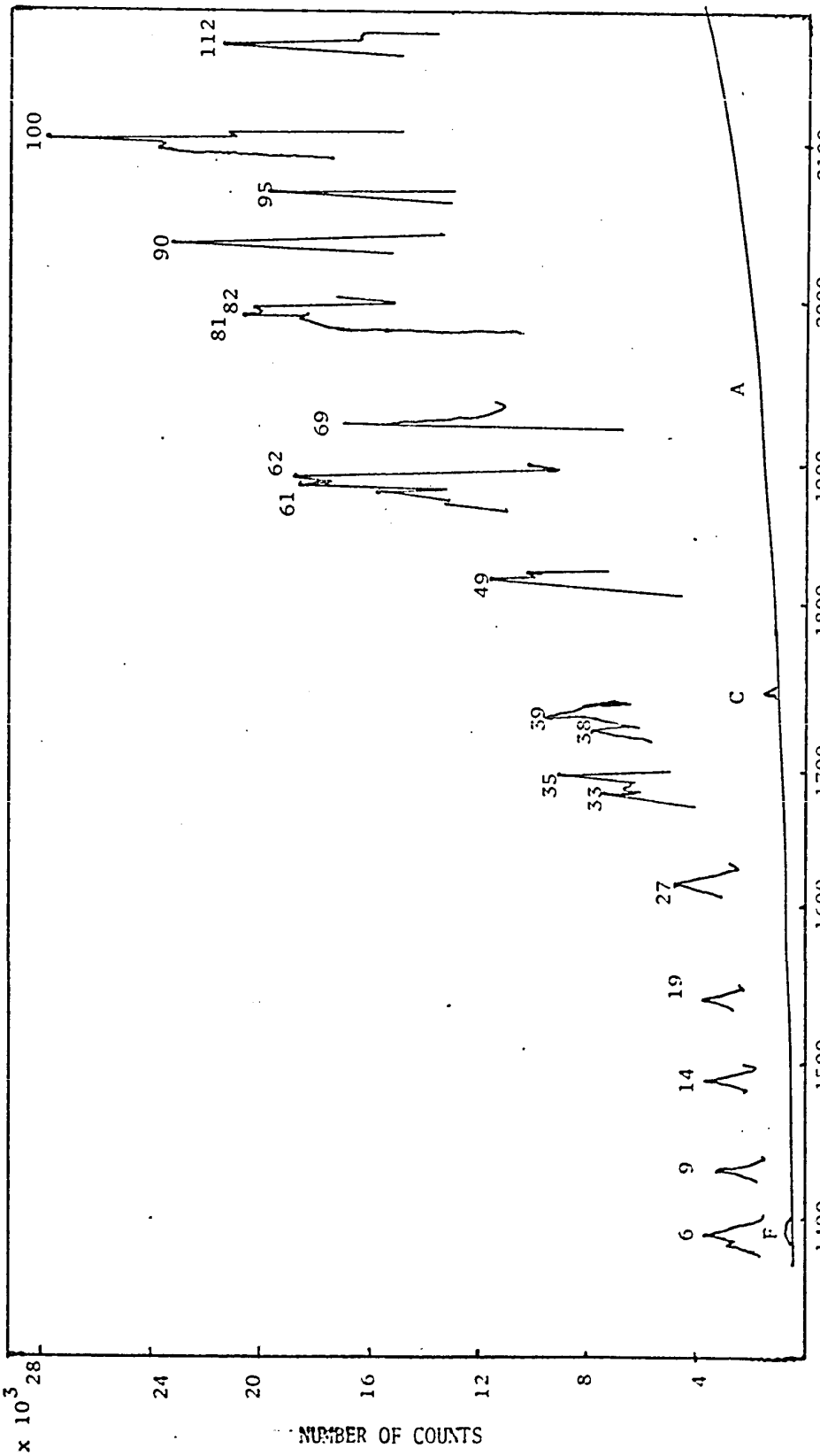
x 10^3
28
24
20
16
12
8
4
NUMBER OF COUNTS
1400
1500
1600
1700
1800
1900
2000
2100
PROTON ENERGY (KEV)
112
100
95
90
81
82
69
62
61
49
39
38
35
33
27
19
14
9
6
F
C
A

Figure 6.

Table 1-1, 1-2, 1-3 and 1-4 for $^{63}Cu(p, \gamma)^{64}Zn$ Reaction:

Resonance bombarding energies E_p = ±2 Kev

and compound-nucleus energies E_x = ±5 Kev

with a Q-value of 7706.2 ± 5 Kev.

TABLE 1-1

No.	E_p(Kev)	E_x(Kev)
1	1322	9008
2	1328	9013
3	1334	9019
4	1362	9047
5	1378	9063
6	1381	9066
7	1406	9090
8	1415	9099
9	1426	9110

Table 1-1 continued:

10	1440	9124
11	1449	9133
12	1467	9150
13	1479	9162
14	1486	9169
15	1495	9178
16	1512	9195
17	1524	9206
18	1531	9213
19	1542	9224
20	1552	9234
21	1556	9238
22	1566	9248
23	1583	9264
24	1597	9278

TABLE 1-2

No.	E_p(Kev)	E_x(Kev)
25	1600	9281
26	1606	9287
27	1621	9302
28	1643	9324
29	1650	9330
30	1652	9332
31	1661	9341
32	1668	9348
33	1680	9359
34	1684	9364
35	1693	9373
36	1705	9385
37	1710	9390
38	1721	9400
39	1733	9412
40	1740	9419
41	1749	9428
42	1760	9439

Table 1-2 continued:

43	1771	9450
44	1775	9453
45	1780	9458
46	1785	9463
47	1791	9469
48	1798	9476
49	1817	9495
50	1820	9498
51	1825	9502
52	1833	9511
53	1838	9515
54	1848	9525
55	1853	9530
56	1857	9534
57	1861	9538

TABLE 1-3

No.	E_p(Kev)	E_x(Kev)
58	1863	9540
59	1867	9544
60	1873	9550
61	1877	9554
62	1881	9558
63	1891	9568
64	1895	9572
65	1898	9575
66	1904	9580
67	1908	9584
68	1911	9587
69	1922	9598
70	1934	9610
71	1937	9613
72	1942	9618
73	1947	9623

Table 1-3 continued:

74	1949	9625
75	1953	9629
76	1957	9633
77	1964	9640
78	1968	9643
79	1973	9648
80	1982	9657
81	1986	9661
82	1988	9663
83	1997	9672
84	2000	9675
85	2005	9680
86	2014	9689
87	2017	9692
88	2021	9695
89	2024	9698
90	2028	9703

TABLE 1-4

No.	E_p(Kev)	E_x(Kev)
91	2038	9712
92	2044	9718
93	2054	9728
94	2056	9730
95	2062	9736
96	2073	9746
97	2076	9750
98	2079	9753
99	2091	9764
100	2094	9767
101	2099	9772
102	2104	9777
103	2108	9781
104	2114	9787
105	2117	9790
106	2121	9754
107	2126	9790

Table 1-4 continued:

108	2130	9803
109	2135	9808
110	2141	9814
111	2144	9817
112	2156	9829
113	2167	9839
114	2173	9845
115	2176	9848
116	2180	9852

CHAPTER IV NUCLEAR LEVEL DENSITY

(A) Theory of Nuclear Level Density.

An experimental feature of the nuclear level density is its rapid increase with excitation energy, especially in medium weight and heavy elements. Also, the level density of the even-even nuclei is much lower than that of odd-odd nuclei, especially in the neighbourhood of magic-nuclei. This effect is particularly marked in the case of the doubly magic nucleus ^{208}Pb.

Several workers have sought to explain these results on the basis of theoretical models. Most considerations of the nuclear level density at elevated energies have been based on the Fermi gas model, first applied to this problem by Bethe[3]. He started with idea of replacing all the nucleon-nucleon interactions by an average potential which serves mainly to hold the nucleus together. The nucleons occupy the single-particle states of this potential as non-interacting particles while obeying the Pauli exclusion principle; the total energy of a nuclear level is then just the sum of the energies of the individual particles.

By assuming that the nucleons are free particles in a spherical well of radius $R = r_0 A^{1/3}$, Bethe showed that the nuclear level density ρ is essentially given by

$$\rho = C \exp(2\sqrt{aU}) \quad . \tag{1}$$

Where A is the nucleon number, U is the excitation energy, a is a parameter dependent upon A and C is a constant.

This simple formula gave a good account of the gross features of experimentally observed level densities, namely their rapid rise with both energy and nucleon number. But as experimental data accumulated, particularly on the low-lying levels and the neutron resonances it became clear that the actual level density behaved in a more complicated way. Especially large deviations from the Bethe formula occur near closed shells.

Later, the mathematical formulation of the level density was given by Van Lier and Uhlenbeck[4], Lang and LeCouteur[5], Newton[6], Cameron[7], Ericson[8] and A. Gilbert[9], among others. These formulae will be outlined in here.

The constant spacing model

Ericson has derived a method of calculating the level density in the Fermi gas model in which the densities of neutron and proton states are constant. A typical approximate result is obtained of the form

$$\rho(U,J) = \frac{\sqrt{\pi}}{12} \frac{\exp(2\sqrt{aU})}{a^{1/4}\, U^{5/4}} \frac{(2J+1)\exp\left[-\frac{(J+\frac{1}{2})^2}{2\sigma^2}\right]}{2\sqrt{2\pi}\,\sigma^3} \qquad (2a)$$

where $\rho(U,J)$ is the density (in Mev^{-1}) of levels of given angular momentum J (both parities included) at an energy $U = E - E_0$ (U is excitation energy and E_0 is the ground state energy), a is a parameter, and σ^2 is mean square deviation. The observable level density is

$$\rho(U) = \sum_J \rho(U,J) \simeq \frac{\sqrt{\pi}}{12} \frac{\exp(2\sqrt{aU})}{a^{1/4}\, U^{5/4}} \frac{1}{\sqrt{2\pi}\,\sigma} \qquad (2b)$$

The total level density is

$$W(U) = \sum_J (2J+1)\, \rho(U,J) = \frac{\sqrt{\pi}}{12} \frac{\exp\,(2\sqrt{aU})}{a^{1/4}\, U^{5/4}} \qquad (2c)$$

which includes levels degenerate in M, the magnetic quantum

number (there are 2J+1 of these for every value of J).

The parameter a is given by the relation

$$a = 2\left(\frac{\pi}{3}\right)^{4/3} \frac{M r_o^2}{\hbar^2} A \qquad (3)$$

where M is the mass of a nucleon. For $r_o = 1.2f$, $a = A/13.5$

For $r_o = 1.5f$, $a = A/8.7$ Mev^{-1}

(a) The methods of Newton and Cameron

The validity of the constant-spacing formula, eq(2), depends on the density of single-particle states being a slowly varying function of energy. In the Mayer-Jensen shell model (10), however, the outstanding feature of the single-particle spectrum is the presence of gaps at magic numbers, notably at 28, 50, 82 and 128 particles. One would have every reason to expect actual level density to depart significantly from eq. (2). The reason comes from the fact that the pairing energy which depresses the ground states of Nuclei containing even numbers of Neutrons or protons is a co-operative phenomenon which cannot be contained in the model of a Fermi gas of non-interacting particles. In order to stay

within the framework of the constant spacing formula, the excitation energy and parameter a had to be corrected:

$$U = E - p(Z) - p(N) \qquad (4)$$

where E is the total excitation energy, while P(Z) and P(N) are the pairing energies of protons and neutrons respectively. Modifying Newton's formulation slightly, Lang calculated a from

$$a = 0.0748\ (jn + jp + 1) \qquad (5)$$

where jn and jp are effective values of angular momentum for neutrons and protons near Fermi level (tabulated by Newton (6)). The numerical factor is a free parameter, selected by Lang for a best fit with the absolute level density determined near the neutron-binding energy. As jn and jp are roughly proportional to $A^{1/3}$, the over-all calculated dependence of a on A is linear.

(b) The Method of Gilbert and Cameron

The parameter a of eq. (2) was discussed by Gilbert and Cameron. They improved the situation by determing single-particle states from a semi-empirical mass formula. The Coulomb terms were dropped from the mass formula, since raising a proton

to an excited state does not change the electrostatic energy significantly. The pairing energy was also dropped because it represents a collective phenomenon completely outside the scope of the shell model. Since they have used the pairing energies derived from the semi empirical mass formula to remove the difference due to odd-even effects, the use of shell corrections was made to remove the difference between nuclei near and far from closed shells. In Bethe's theory where a/A is constant, Gilbert and Cameron found a connection between a/A and S, the shell correction.

For undeformed nuclei, $A \geq 30$, the equation is

$$a/A = 0.00917S \pm 0.142 \qquad (6a)$$

For deformed nuclei, $A \geq 30$, the equation is

$$a/A = 0.00917S \pm 0.12 \qquad (6b)$$

The U is defined as in eq. (4).

In the above method, the excitation energy U must be greater than $(2.5 + 156/A)$ Mev

(B) Analysis of Nuclear Level Density

The theoretical and experimental results of the level density of ^{64}Zn are shown in Figure 7, in which, for all

the theoretical methods, U was corrected for the pairing energy. In the $^{63}Cu\ (p,\gamma)^{64}Zn$ reaction, the U in eq(4) is

$$U = E - p(Z)$$
$$= E - 1.06\ \text{Mev}$$

that is because the contributions of the P(N) values to the Q value cancel. The parameter a of Bethe's theory was calculated by eq(6a) which was given by the method of Gilbert and Cameron. The three theoretical calculations of level density were normalized to the level density of the first energy interval of the experimental result.

Figure 7. The experimental result of the Nuclear Level Density of ^{64}Zn comparision with theoretical calculation by Bethe, Newton and Cameron, and Gilbert and Cameron.

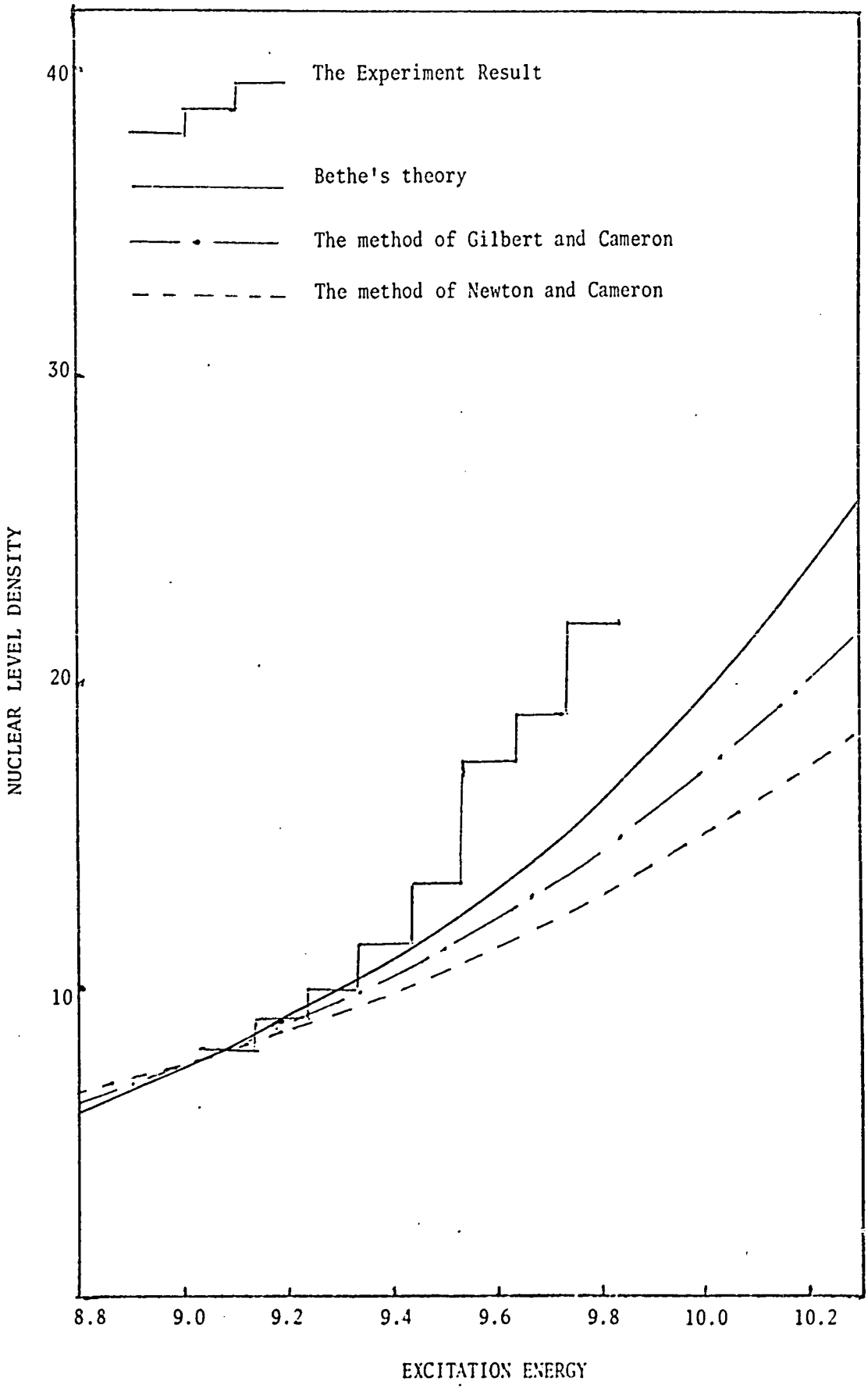
The Experiment Result
Bethe's theory
The method of Gilbert and Cameron
The method of Newton and Cameron
NUCLEAR LEVEL DENSITY
40
30
20
10
8.8
9.0
9.2
9.4
9.6
9.8
10.0
10.2
EXCITATION ENERGY

CHAPTER V ISOBARIC ANALOGUE STATES

(A) Theory of Isobaric Analogue States.

The excitation of isobaric states in (p,n) reactions was first observed by Anderson and Wong[11] who in a study of ^{51}V (p,n)^{51}Cr reaction at proton energy up to 18.5 Mev found peaks with Q-values equal to the coulomb energy difference between the target ^{51}V and the residual nucleus ^{51}Cr. These peaks were interpreted as being due to neutrons leaving the residual nucleus in a state which is the isobaric analogue of the ground state of the residual nucleus [12,13]. An explanation in terms of an isobaric spin dependent potential in the optical model has been given by Lane[14,15].

The hypothesis upon which the Isospin theory is based on is that the nuclear forces are independent of the nucleon charge. Because of the Exclusion Principle, the charge independence symmetry refers only to the channels with anti-symmetric space-spin wave functions, that is, singlet spin (S = 0) and even orbital angular momentum (^1S, ^1D,-) or triplet spin (S = 1) and odd orbital symmetry (^3p, ^3F,--) . In these channels, the interaction is assumed to be the

the same for nn, np, and pp systems. The symmetry channels ^3S, ^1P, ^3D -- are permitted only for the np system.

As is well known from the quantal description of spin, any 2 X 2 matrix can be expressed in terms of linear combinations of the unit matrix and the three pauli matrices. It is therefore possible to express the operators in Isobaric space in terms of the isospin matrices

$$\tau_x = \begin{pmatrix} 0 & 1 \\ 1 & 0 \end{pmatrix} \quad \tau_y = \begin{pmatrix} 0 & -i \\ i & 0 \end{pmatrix} \quad \tau_z = \begin{pmatrix} 1 & 0 \\ 0 & -1 \end{pmatrix} \tag{7}$$

for the individual nucleons.

From the matrices eq(7), the isobaric spin operator is obtained

$$t = \frac{1}{2}\tau \tag{8}$$

whose components obey the commutation relations for components of an angular momentum vector. Since $(t)^2 = \frac{3}{4}$, the nucleon has the total isospin $t = \frac{1}{2}$ and the z-components $M_t = \tau_z = +\frac{1}{2}$ (for neutron) and $-\frac{1}{2}$ (for proton)

For systems with two or more nucleons, the isospin may be coupled to a total

$$\bar{T} = \Sigma_k \bar{t}_k \tag{9}$$

with the component

$$M_T = T_z = \frac{1}{2}(N - Z) \tag{10}$$

where N is total number of neutrons and Z is total number of protons.

The isobaric invariance is violated by the electromagnetic interaction. The symmetry-breaking effects in the nuclear structure are partly associated with the coulomb force (and magnetic force) between nucleons. Additional effects arise from the neutron-proton mass difference and small charge-dependent components in the strong nucleonic interactions which appear to be associated with the electromagnetic structure of the nucleons. For the lightest nuclei, these effects are relatively small and can be rather accurately treated as perturbations which mainly act to give small energy splittings between the isobaric multiplets. In heavier nuclei, the coulomb field may become very strong, reaching values of the order of 20 Mev inside the heaviest nuclei. Thus, for a long-time, it was expected that the isobaric symmetry might be of little significance in heavy nuclei. The discovery of well-defined isobaric multiplet structure has revealed, however, that the

strong Coulomb interactions are rather ineffective in breaking the isobaric symmetry.

The validity of the T quantum number in heavy nuclei may be understood from the fact the coulomb field varies rather slowly over the nuclear volume. Thus the wave functions of the individual protons are only little affected and the main result of the coulomb field is to add to the nuclear energy a term depending on the number of protons (that is, on M_T) without violating the T quantum number.

Swamy and Green[16] have used independent-particle model wave functions to calculate the coulomb energy. For a nucleus of charge Z and radius R, the coulomb energy is

$$E_c = \frac{3}{5} \frac{e^2 Z^2}{R} \left(1 - \frac{C}{Z^{2/3}}\right)$$

$$= 0.70 \frac{Z^2}{A^{1/3}} \left(1 - 0.764\, Z^{-2/3}\right) \qquad (11)$$

where $c = 0.764$ for $Z>10$. And $R = 1.75\, A^{1/3}$ for $A \geq 40$. The coulomb energy difference between nuclei of charges $Z + 1$ and Z is given to a good approximation by

$$\Delta E_C = \frac{3}{5} \frac{e^2}{R} \left[(2Z+1) - \frac{4}{3}C \left(Z + \frac{1}{2}\right)^{1/3}\right]$$

$$= 0.70 \frac{1}{A^{1/3}} \left[(2Z+1) - 1.019 \left(Z + \frac{1}{2}\right)^{1/3}\right] \qquad (12)$$

Eq.(12) is without a neutron-proton mass correction.

(B) Analysis of Isobaric Analogue States

The isospin of ^{64}Zn, its isobar ^{64}Cu, and the target ^{63}Cu in the ground state are shown in Table 2.

TABLE 2

NUCLEUS	ISOSPIN T	M_T
$^{64}_{29}Cu$ 35	3 (g.s)	3
$^{64}_{30}Zn$ 34	3,2(g.s)	2
$^{63}_{29}Cu$ 34	$\frac{5}{2}$ (g.s)	$\frac{5}{2}$

The T = 3 level in ^{64}Zn which has been observed in the proton resonance reaction with ^{63}Cu was shown in Figure 8, in which the coulomb energy difference was calculated by the semi-empirical method. The coulomb energy difference between ^{66}Cu and ^{66}Zn after neutron-proton mass correction, is 9.51 ±0.03 Mev

which was given by Harchol etc.[20] and which, together with eq.(12), was used to calculate the coulomb energy difference between ^{64}Cu and ^{64}Zn. The E_c (^{64}Cu ~ ^{64}Zn) was calculated by

$$\frac{\Delta E_c\ (^{64}Cu - {}^{64}Zn)}{\Delta E_c\ (^{66}Cu - {}^{66}Zn)} = \frac{(A\ 66_{Zn})^{1/3}}{(A\ 64_{Zn})^{1/3}}$$

$$\Delta E_c\ (^{64}Cu - {}^{64}Zn) = \frac{(66)^{1/3}}{(64)^{1/3}} \times (9.51 + 0.782)$$

$$= 10.398 \pm 0.03 \text{ Mev}$$

After neutron-proton mass correction, the coulomb energy difference between ^{64}Cu and ^{64}Zn is

$$\Delta\varepsilon_c\ (^{64}Cu - {}^{64}Cu) = \Delta E_c\ (^{64}Cu - {}^{64}Cu) - (M_n - M_p)C^2$$

$$= 10.398 - 0.782 = 9.616 \pm 0.03 \text{ Mev.}$$

The value of $E_p = 1.700 \pm 0.03$ Mev, which corresponds to the excitation energy $E_x = 9.406 \pm 0.03$ Mev in ^{64}Zn, is an analogue state of ^{64}Cu. In comparison with the level scheme ^{64}Cu with ^{64}Zn which was obtained by this work and which was

shown in Figure 9, the best choice within the error range for the Analogue state of the ground state of ^{64}Cu is 9.3994 Mev, and the next higher analogue states are 9.554, 9.598, 9.672, 9.736, and 9.753 Mev which correspond to the excitation energies of 0.159, 0.205, 0.278, 0.343 and 0.362 Mev in ^{64}Cu respectively.

The excellent agreement of the level scheme of ^{64}Zn with that of ^{64}Cu (shown in Figure 9) determines the experimental result of the Coulomb energy difference between ^{64}Cu and ^{64}Zn, which is 9.604 ± 0.005 Mev.

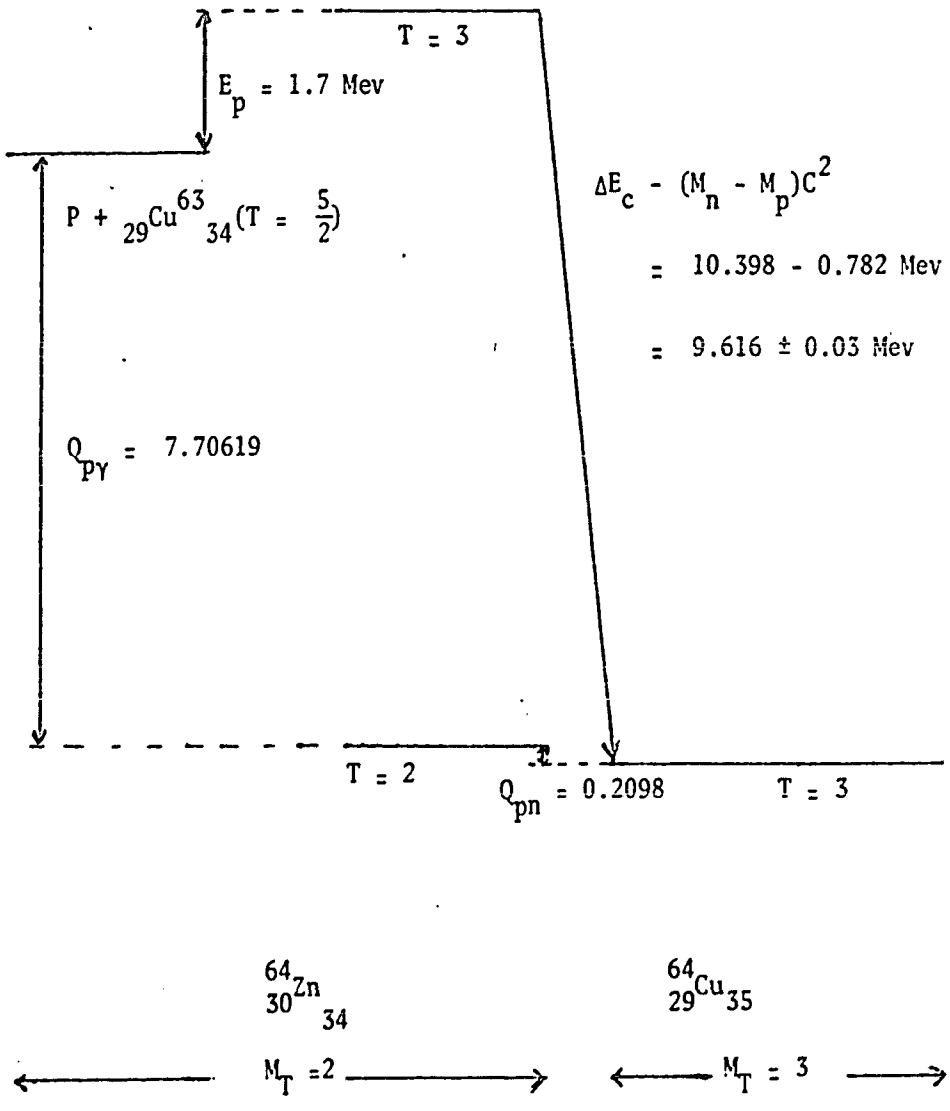

Figure 8 The Level Scheme of the T =3 multiplet. The T=3 state in ^{64}Zn is an analogue state of the ground state of ^{64}Cu.

Figure 9 Some energy levels in ^{64}Zn which were from strong resonance of $^{63}Cu(p, \gamma)^{64}Zn$ and were found to be the analog states of ^{64}Cu.

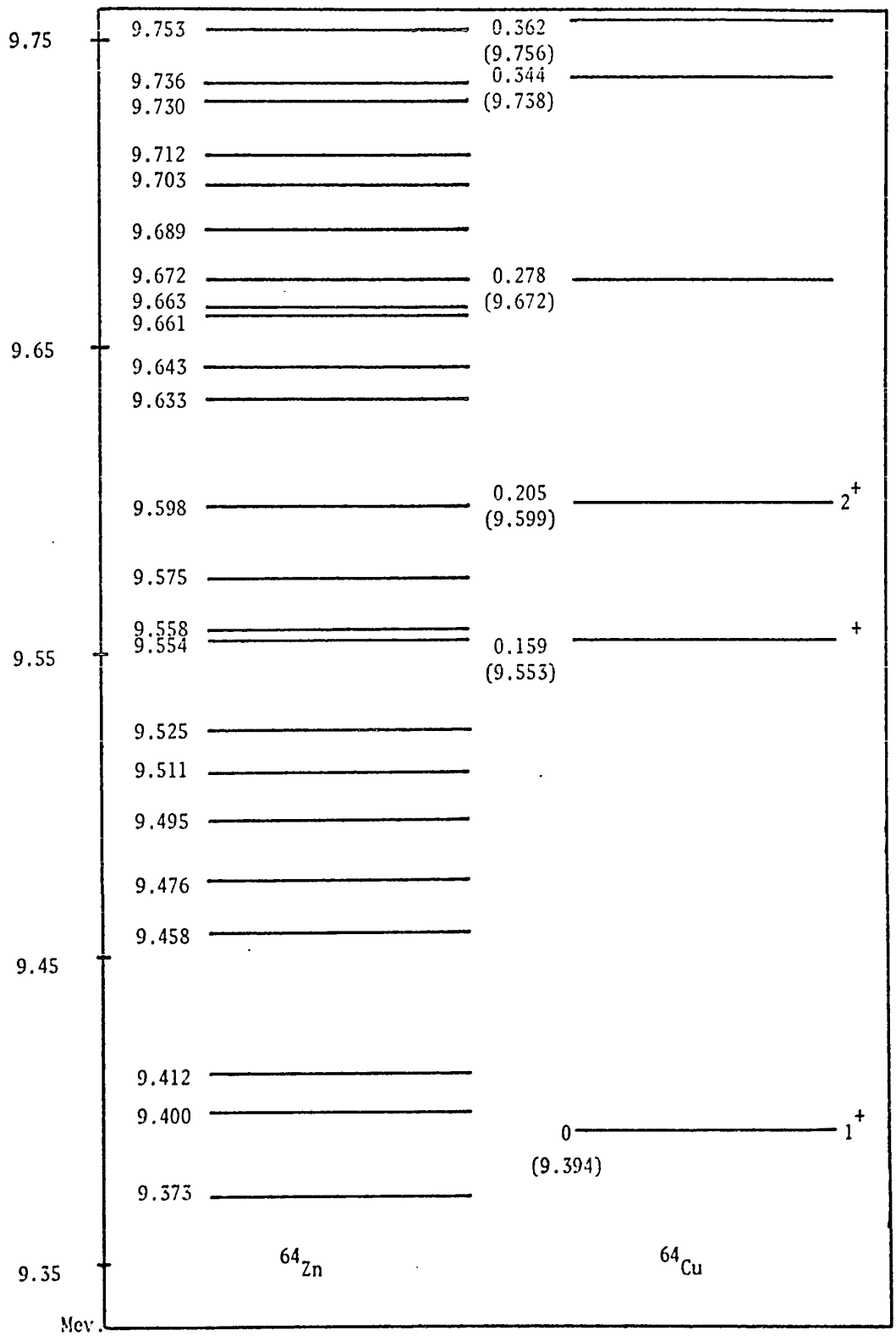
9.75
9.65
9.55
9.45
9.35
Mev.
9.753
9.736
9.730
9.712
9.703
9.689
9.672
9.663
9.661
9.643
9.633
9.598
9.575
9.558
9.554
9.525
9.511
9.495
9.476
9.458
9.412
9.400
9.373
0.362
(9.756)
0.344
(9.738)
0.278
(9.672)
0.205
(9.599)
2+
0.159
(9.553)
+
0
1+
(9.394)
64Zn
64Cu

Figure 9.

CHAPTER VI DECAY SCHEME

The gamma-ray spectra of the resonances no. 69, no. 94, and no. 100, which are shown in Figures 10-1, 10-2, 10-3, 12-1, 12-2, 12-3, 14-1, 14-2, and 14-3, were measured at an angle of 90^{o} to the proton beam. The distance between the target and Ge(Li) detector was about 2 cm. The times of measurement for these spectra were 2 hours for resonance no. 69, 3 hours for resonance no. 94, and 1 hour for resonance no. 100 with a beam current of 12 microamperes.

(A) Spectrum Analysis

The interaction of gamma-rays with the Ge(Li) detector crystal produced three main types of phenomena: Compton effect, Photoelectric effect and Electron-positron pair production. The probability of interaction by each of these processes depended on the gamma-ray energy. At low energies, photoelectric absorption was the dominant process and gave rise to a single peak or photopeak corresponding to the absorption of the full gamma-ray energy. Compton scattering was present at all energies

and resulted in a broad distribution beginning at slightly below the full energy peak and extending down to zero energy. It was also possible for the Compton scattered photon to be absorbed in the crystal and, in this way, contribute to the full energy peak. The relative importance of the latter process depended on gamma-ray energy and crystal size. At gamma-ray energies above 1.02 Mev electron-positron pair production became energetically possible. The probability for interaction by pair production increased with increasing energy while that for photoelectric absorption decreased. The probability for interaction by Compton scattering also decreased with increasing energy but less rapidly than it did for photoelectric absorption. At energies above approximately 2.5 Mev three other peaks, in addition to the photopeak, were observed. These peaks resulted from the interaction of the photons by pair production in either the crystal or the surrounding material. The positrons resulting from the pair-production process annihilated with electrons producing two 0.511 Mev photons. If the positrons were produced in the crystal, one or both of the annihilation photons could escape from the crystal. If only one photon escaped, a single peak of energy 0.511 Mev less than the photopeak was produced while if both photons escaped, a peak of energy 1.02 Mev less

than the photopeak was produced. The 0.511 Mev peak resulted from the detection of annihilation radiation produced in the surrounding material and not from the primary interactions in the detector. Thus, the response to or "Line shape" of a given gamma-ray was due to the crystal dimensions, a combination of the above three basic processes, and the effect of electronic noise.

(B) Result

The spectra of resonances no. 69, no. 94, and no. 100 were identified. The data and its comparison with ^{64}Ga (β^+) ^{64}Zn decay[21-23] and $^{64}Zn(p,p'\gamma)$ ^{64}Zn reaction[24] are shown in table 3-1,3-2, and 3-3. The data was also used to construct the level scheme shown in Figure 11, 13, and 15.

Comments on the properties of some of the individual levels follow below.

The 9769 Kev, 9732 Kev, and 9600 Kev levels. These three levels which were the energies of resonances no. 100, no. 94, and no. 69 respectively had transitions to the ground state and to the 991.7 Kev, 1799.8 Kev, and 2305.3 Kev levels. The 9732 Kev level also had a transition to the 2789 Kev level. The branching ratio has shown that these three resonances favored the transition to the 2^+ level. The experimental Q-value, which was a mean value based on these measured energies of the ground state and the strongest cascades, was 7708 ± 3 Kev. It is in good agreement with the calculated Q-value of 7706 ± 5 Kev.

The 5207 Kev level. This level had transitions to the 3199 Kev level and 3800 Kev level at all three resonances by 2007 Kev and 1406.7 Kev γ-ray. This has not been observed in

^{64}Ga (β^+) ^{64}Zn decay. But the transition from 5207 Kev level to 991.7 Kev level was observed in the $^{64}Ga(\beta^+)$ ^{64}Zn decay by 4215 Kev γ-ray

The 4750 Kev level. This level had a transition to the 3002 Kev level at resonance no. 100 by 1747.6 Kev γ-ray. By comparison the ^{64}Ga (β^+) ^{64}Zn decay had transitions from 4750 Kev level to the ground state.

The 4140 level. The transition from this level to the 3370 Kev level has been observed at resonance no. 100 by the weak 770.4 Kev γ-ray. No transition from this level to the ground state was observed, but the 4140 Kev γ-ray was observed for the ^{64}Zn (p,p'γ) ^{64}Zn reaction.

The 3262.1 Kev level and 3186 Kev level. The transition from the 3262.1 Kev level to the 991.7 Kev level and from the 3186 Kev level to the 991.7 Kev level and to the 1799.8 Kev level were observed both with $^{64}Ga(\beta^+)$ ^{64}Zn decay and with all three resonances considered in the present work. But the transitions from the 3262.1 Kev level and the 3186 Kev level to the ground state which have been observed at $^{64}Ga(\beta^+)$ ^{64}Zn decay were not observed (in the present work).

The 2305.3 Kev level. The angular momentum and spin of this level was 4+ . The transition from this level to the 991.7 Kev, 2+ level was observed at all three resonances of the present work by very strong (87%), 1314.8 Kev γ-ray. But the transition from 2305.3 Kev, 4+ level to the ground state 0+ was also observed at all three resonances of the present work by strong (13%) 2305.3 Kev γ-ray. While the $^{64}Zn(p,p'\gamma)$ ^{64}Zn reaction has only the transition from 2305.3 Kev level to 991.7 Kev level. It may be possible that the low angular moment level mixed with the 2305.3 Kev level.

The 1910.5 Kev, 0+ level, 1799.8 Kev, 2+ level and 991.7 Kev, 2+ level. The observed transitions from the 1910.5 Kev level to 991.7 Kev level, from the 1799.8 Kev level to the ground state and to the 991.7 Kev level, and from the 991.7 Kev level to the ground state were in agreement with ^{64}Ga $(\beta+)$ ^{64}Zn decay and $^{64}Zn(p,p'\gamma)$ reaction.

The 670.4 Kev γ-ray appeared at all three resonances and was from the $^{63}Cu(p,p'\gamma)$ ^{64}Zn reaction.

(1) The spectra shown in Figure 10-1, 10-2. and 10-3 were taken from resonance no. 69. Incident proton energy E_p = 1922 ± 2 Kev.

(2) The spectra shown in Figure 12-1, 12-3 and 12-3 were taken from resonance no. 94. Incident proton energy E_p = 2056 ± 2 Kev.

(3) The spectra shown in Figure 14-1, 14-2 and 14-3 were taken from resonance no. 100. Incident proton energy E_p = 2094.

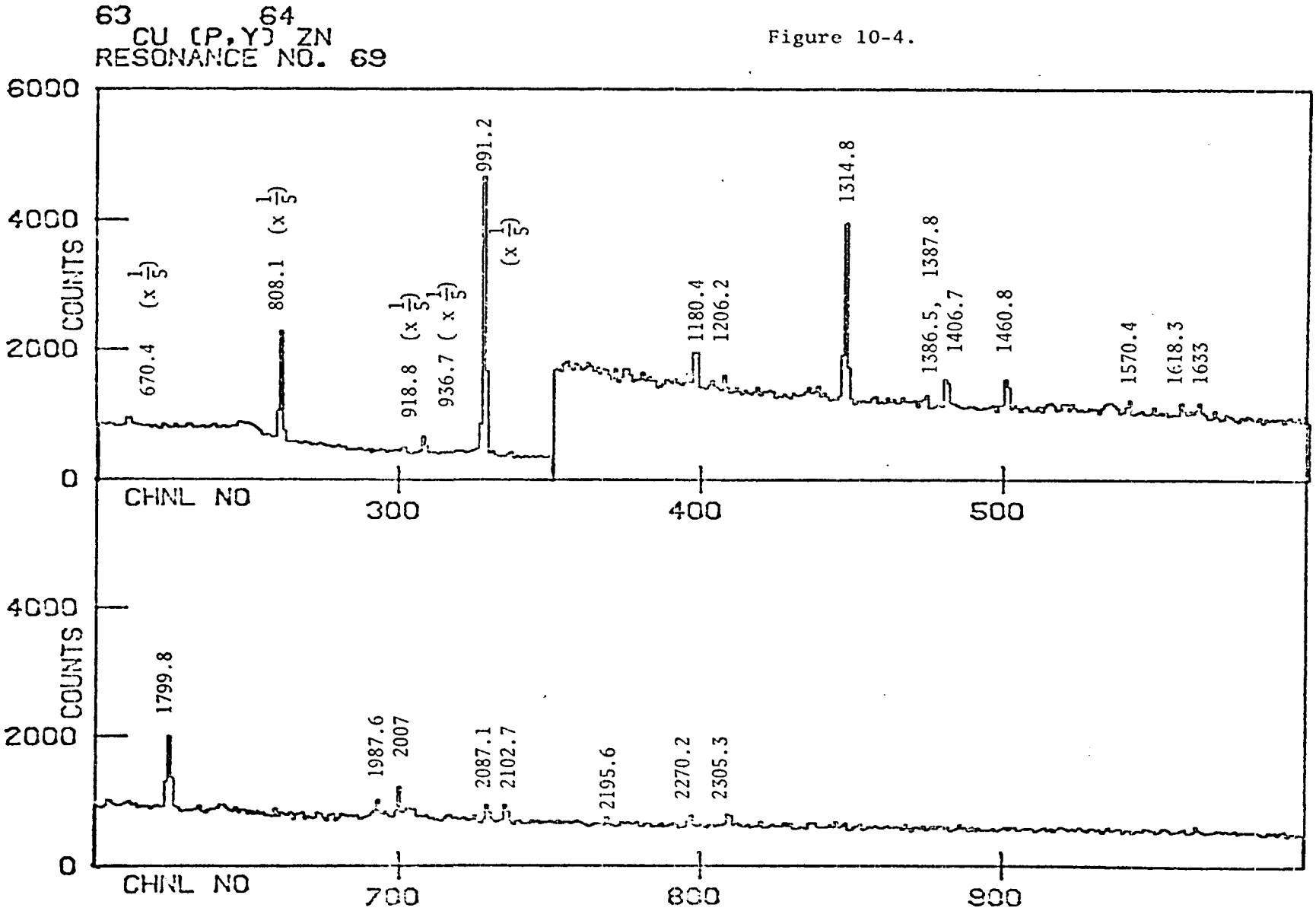
63 64
CU (P,YJ ZN
RESONANCE NO. 69
6000
4000
2000
0
COUNTS
670.4 (x 1/5)
808.1 (x 1/5)
918.8 (x 1/5)
936.7 (x 1/5)
991.2
(x 1/5)
1180.4
1206.2
1314.8
1386.5, 1387.8
1406.7
1460.8
1570.4
1618.3
1633
CHNL NO
300
400
500
4000
2000
0
COUNTS
1799.8
1987.6
2007
2087.1
2102.7
2195.6
2270.2
2305.3
CHNL NO
700
800
900

Figure 10-4.

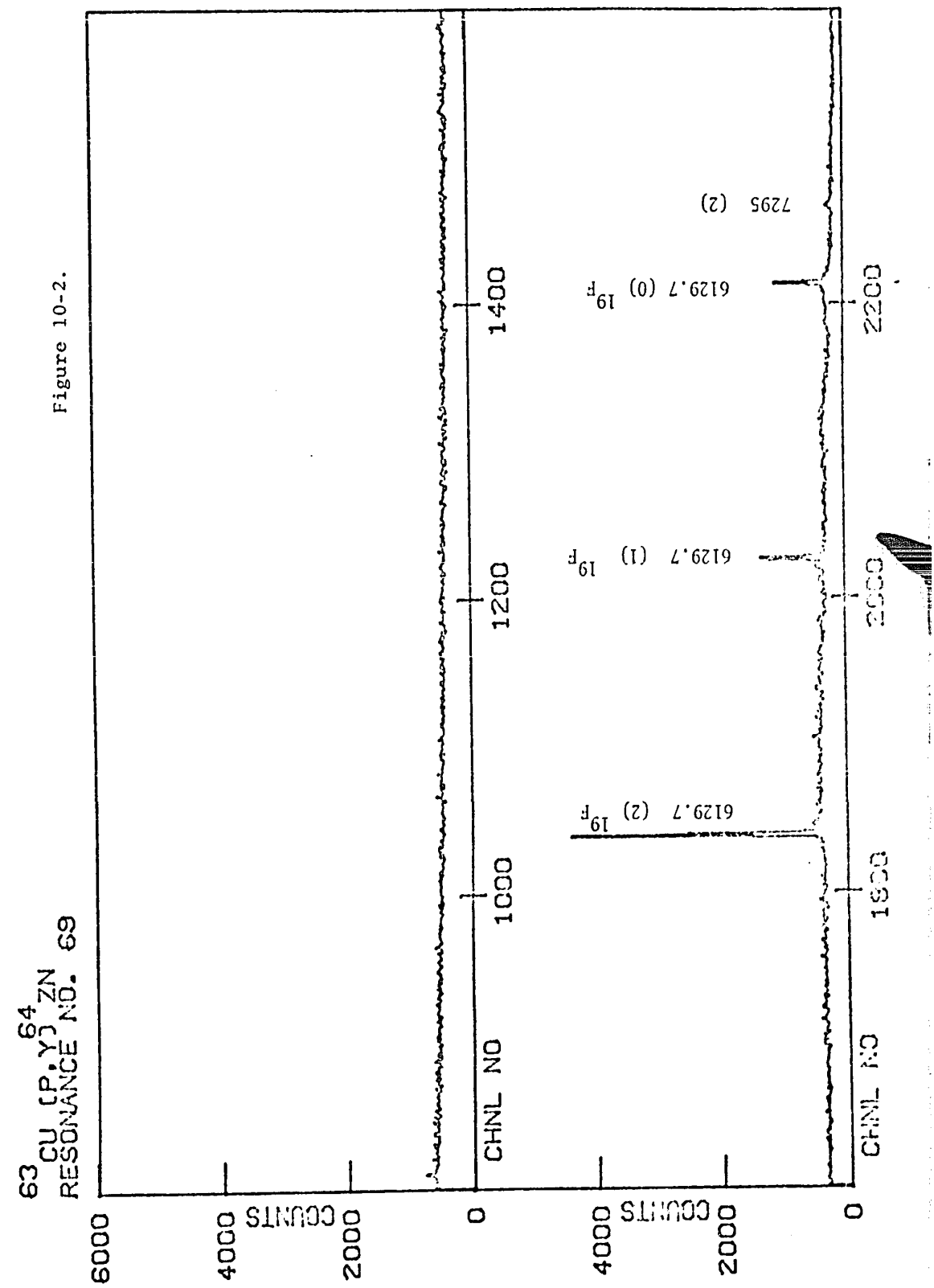
63 CU (P,γ) 64 ZN
RESONANCE NO. 69
6000
4000
2000
0
COUNTS
CHNL NO
1000
1200
1400
6129.7 (2) 19F
6129.7 (1) 19F
6129.7 (0) 19F
7295 (2)
2200

Figure 10-2.

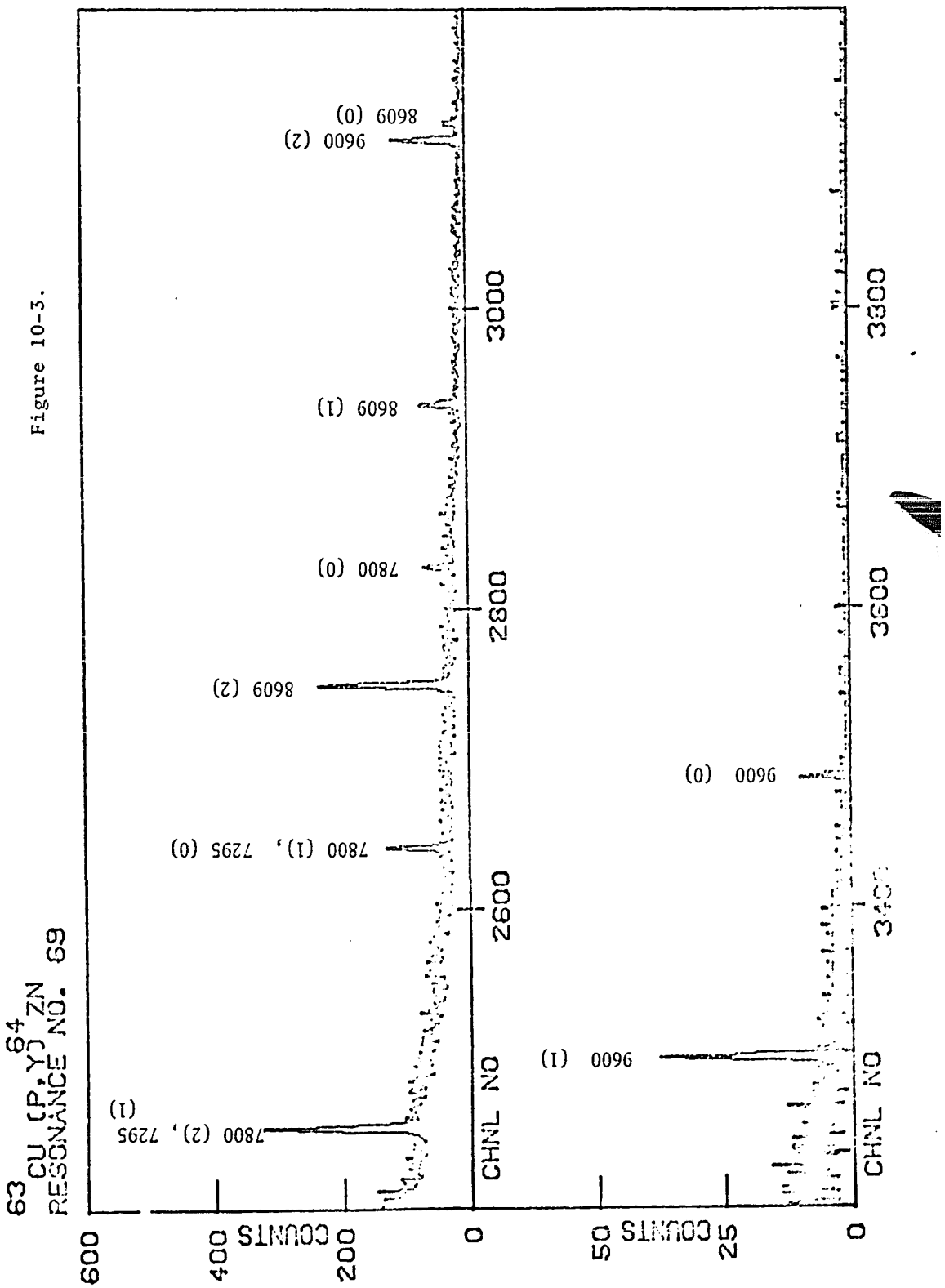
63 CU (P,γ) 64 ZN
RESONANCE NO. 69
7800 (2), 7295 (1)
7800 (1), 7295 (0)
8609 (2)
7800 (0)
8609 (1)
9600 (2)
8609 (0)
9600 (1)
9600 (0)
COUNTS
CHNL NO
600
400
200
0
2600
2800
3000
3300
3600
50
25
0

Figure 10-3.

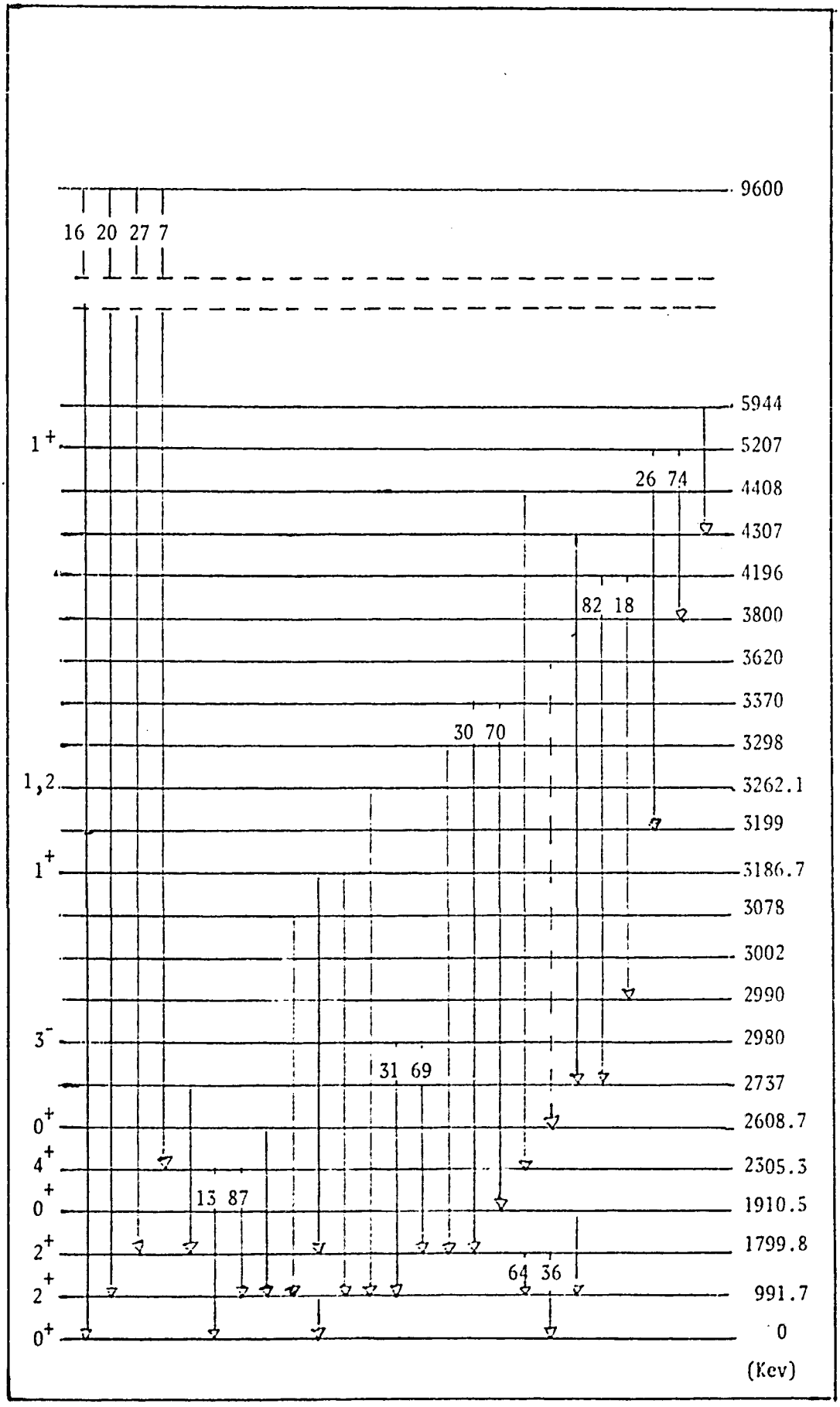

Figure 11 Decay scheme of ^{64}Zn from Resonance no. 69

Figure 12-1.

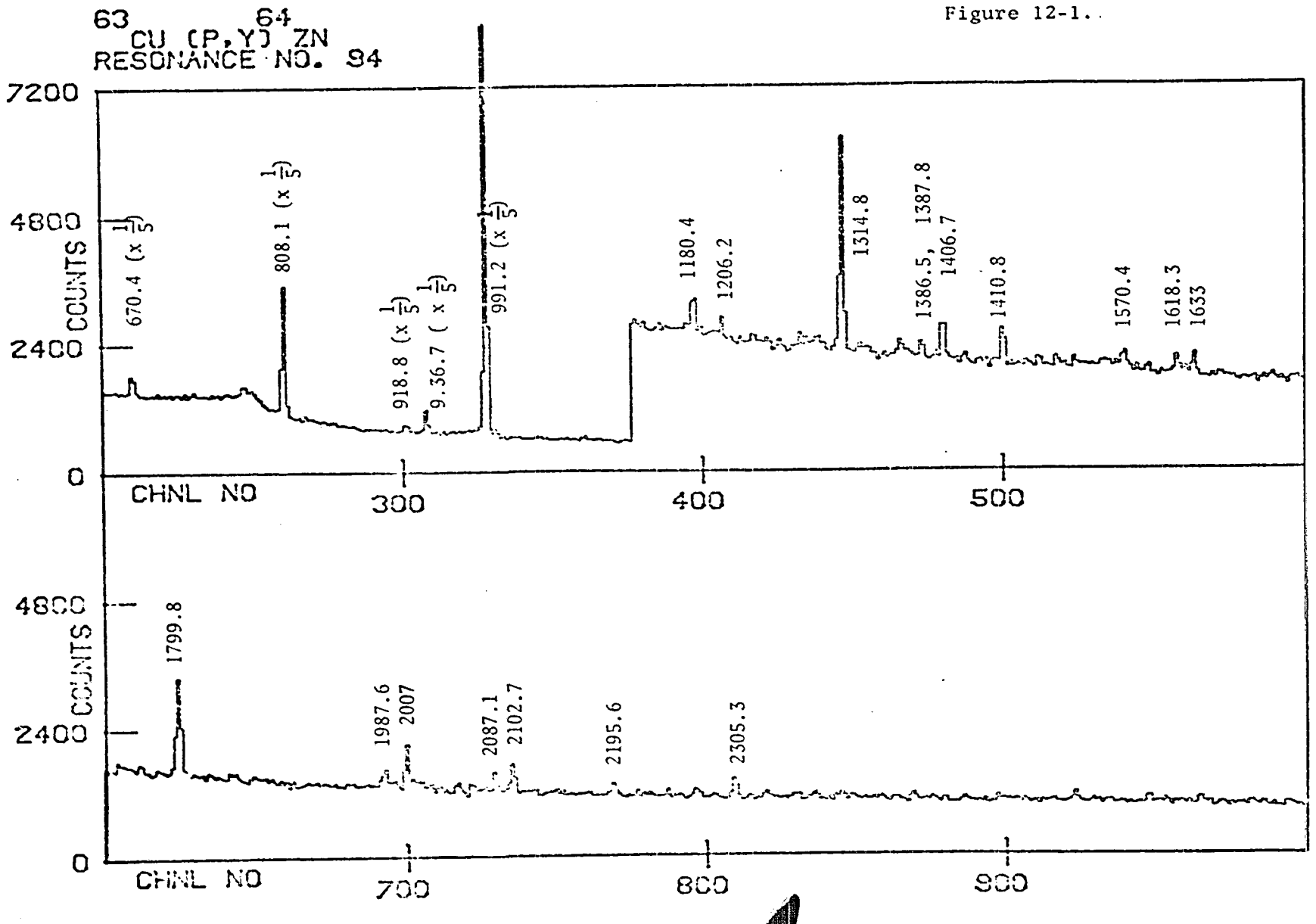
63 64
CU (P,Y) ZN
RESONANCE NO. 94
7200
4800
2400
0
COUNTS
670.4 (x 1/5)
808.1 (x 1/5)
918.8 (x 1/5)
936.7 (x 1/5)
991.2 (x 1/5)
1180.4
1206.2
1314.8
1386.5, 1387.8
1406.7
1410.8
1570.4
1618.3
1633
CHNL NO
300
400
500
4800
2400
0
COUNTS
1799.8
1987.6
2007
2087.1
2102.7
2195.6
2305.3
CHNL NO
700
800
900

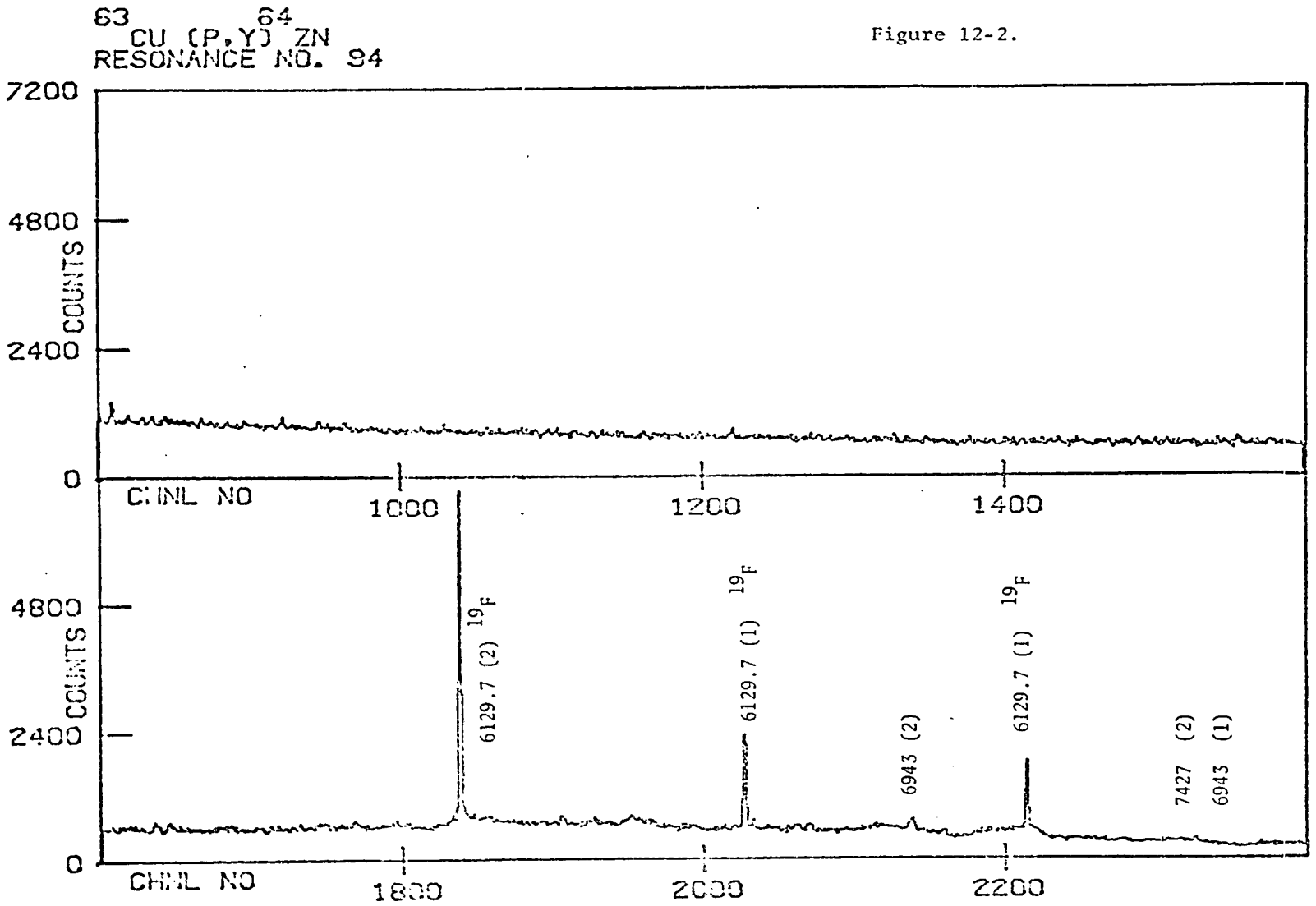
63 64
CU (P,Y) ZN
RESONANCE NO. 94
7200
4800
2400
0
COUNTS
CHNL NO
1000
1200
1400
4800
2400
0
COUNTS
CHNL NO
1800
2000
2200
6129.7 (2) 19F
6129.7 (1) 19F
6943 (2)
6129.7 (1) 19F
7427 (2)
6943 (1)

Figure 12-2.

Figure 12-3.

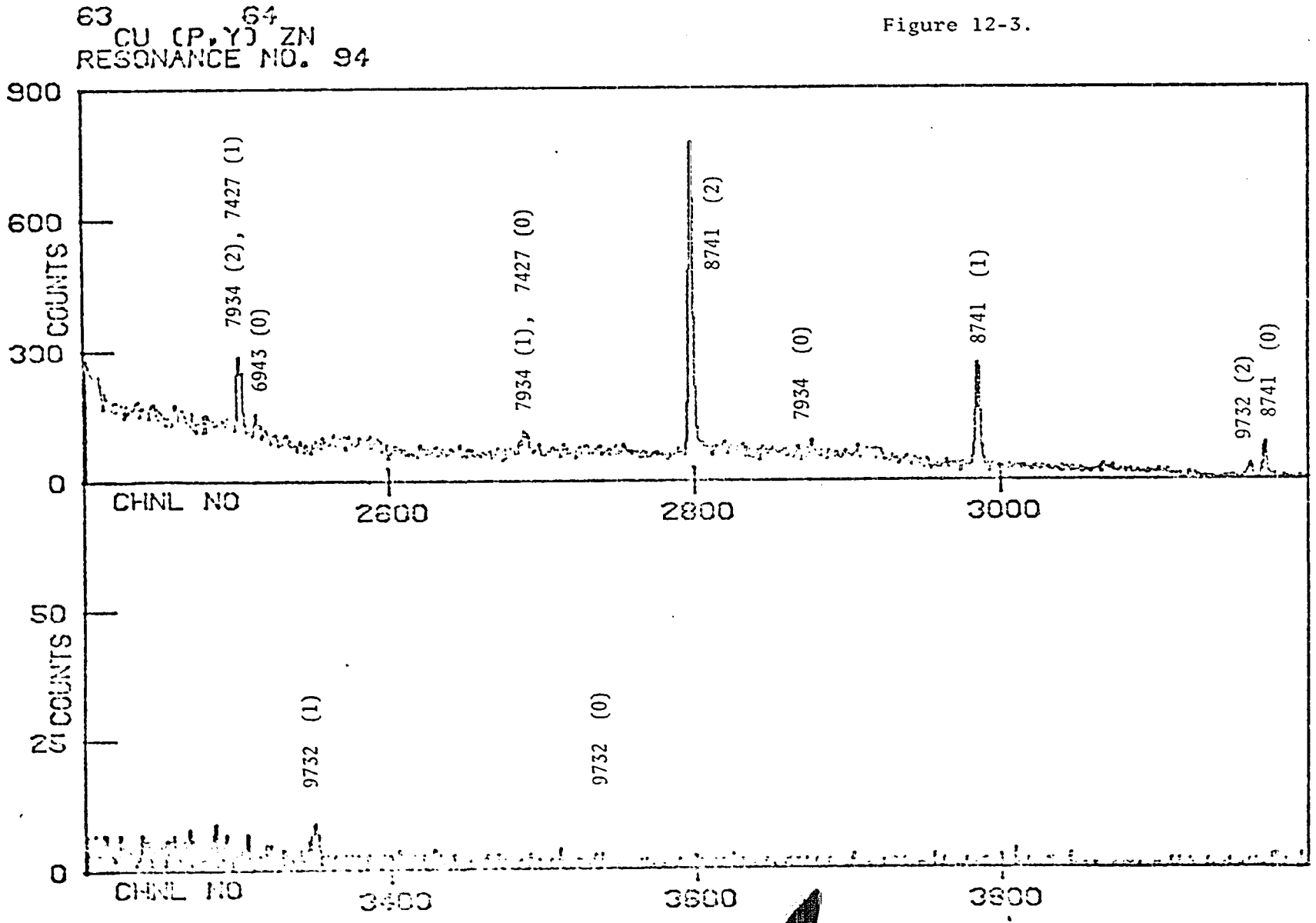
63 64
CU (P,Y) ZN
RESONANCE NO. 94
900
600
300
0
COUNTS
7934 (2), 7427 (1)
6943 (0)
7934 (1), 7427 (0)
8741 (2)
7934 (0)
8741 (1)
9732 (2)
8741 (0)
CHNL NO
2600
2800
3000
50
0
N COUNTS
9732 (1)
9732 (0)
CHNL NO
3400
3600
3800

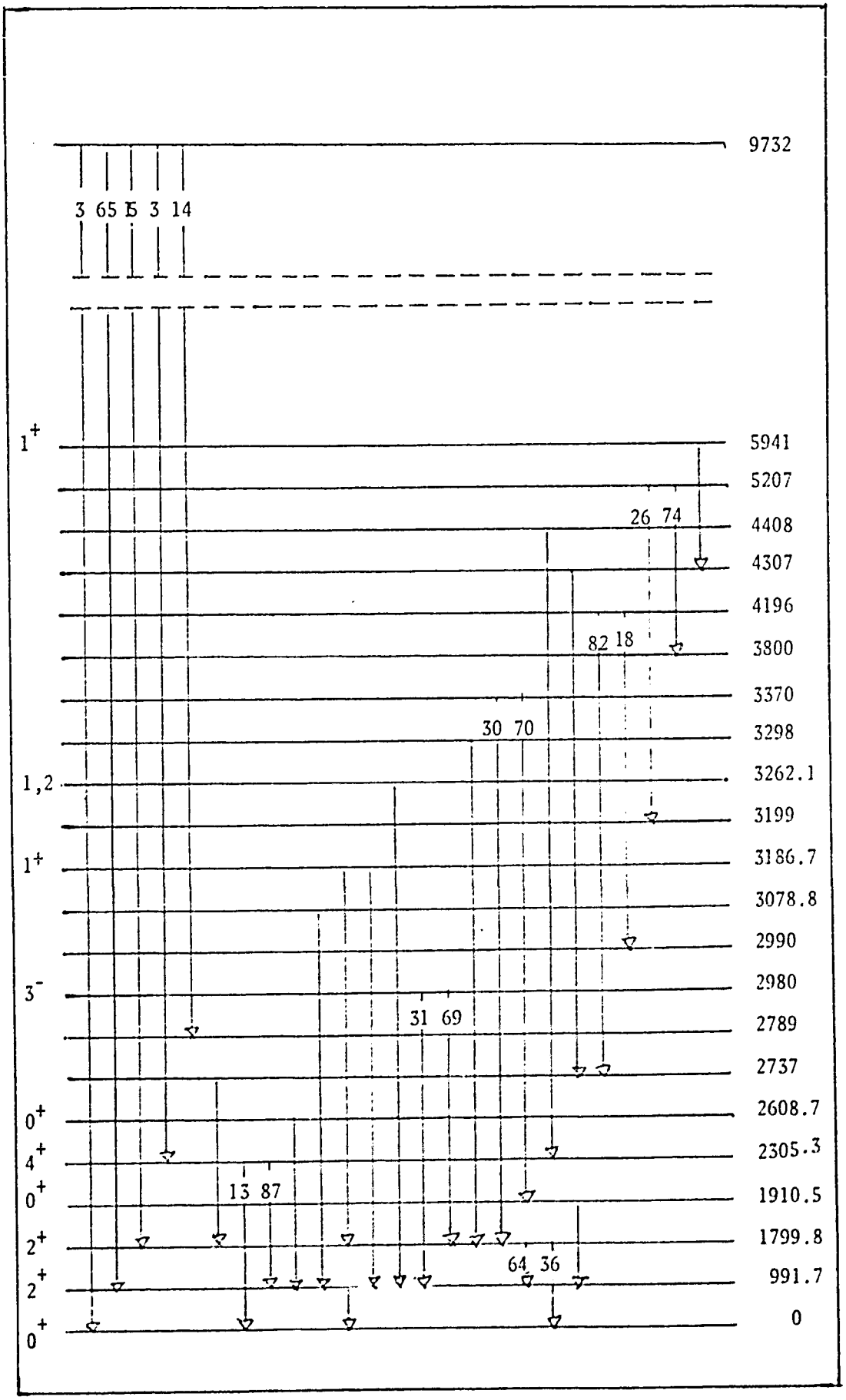

Figure 13 Decay Scheme of ^{64}Zn from resonance no. 94

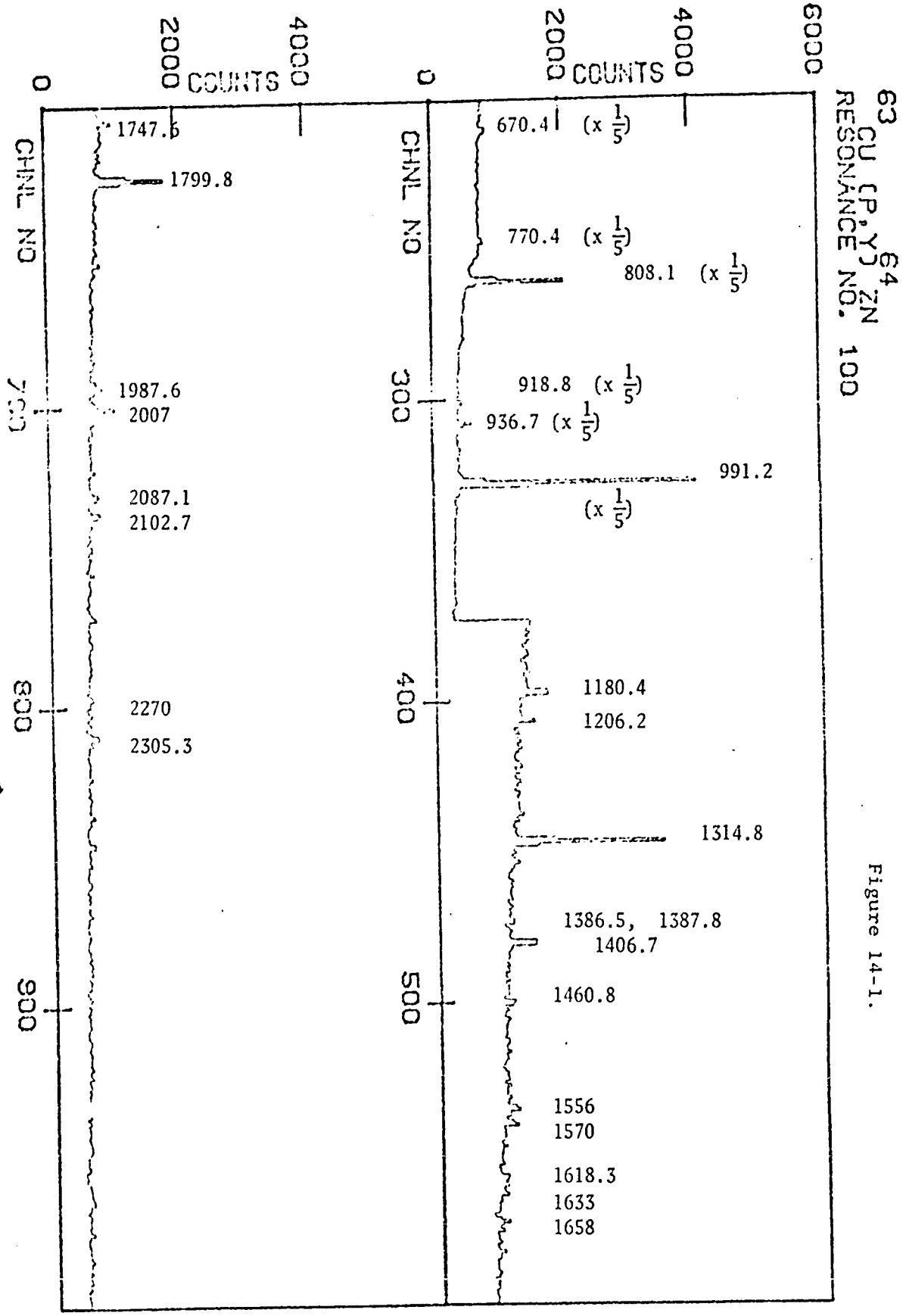
63 CU (P,γ) 64 ZN
RESONANCE NO. 100
0
2000
4000
6000
COUNTS
CHNL NO
700
800
900
300
400
500
1747.6
1799.8
1987.6
2007
2087.1
2102.7
2270
2305.3
670.4 (x 1/5)
770.4 (x 1/5)
808.1 (x 1/5)
918.8 (x 1/5)
936.7 (x 1/5)
991.2
(x 1/5)
1180.4
1206.2
1314.8
1386.5, 1387.8
1406.7
1460.8
1556
1570
1618.3
1633
1658

Figure 14-1.

Figure 14-2.

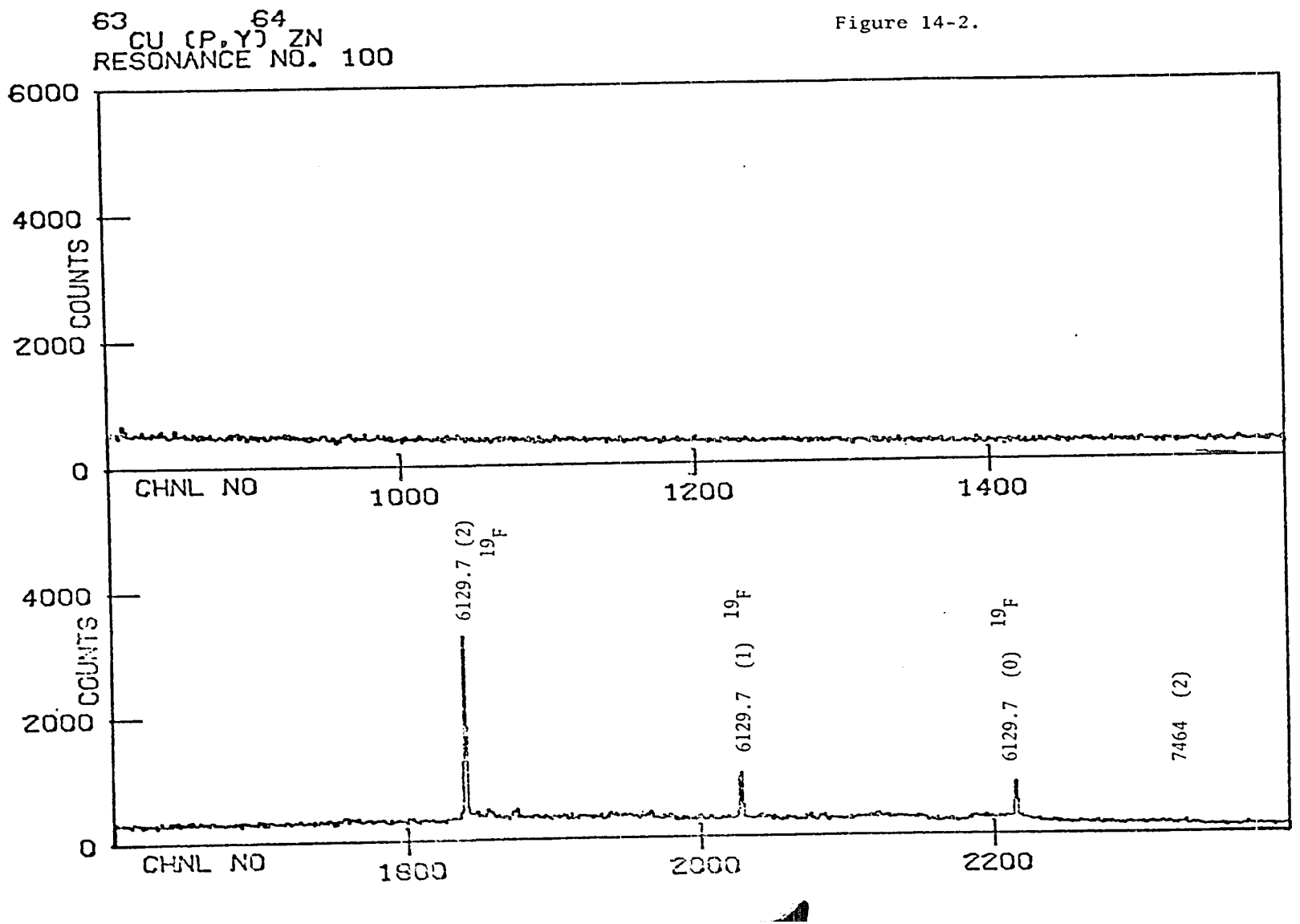
63 64
CU (P,Y) ZN
RESONANCE NO. 100
6000
4000
2000
0
COUNTS
CHNL NO
1000
1200
1400
4000
2000
0
COUNTS
6129.7 (2) 19F
6129.7 (1) 19F
6129.7 (0) 19F
7464 (2)
CHNL NO
1800
2000
2200

Figure 14-3.

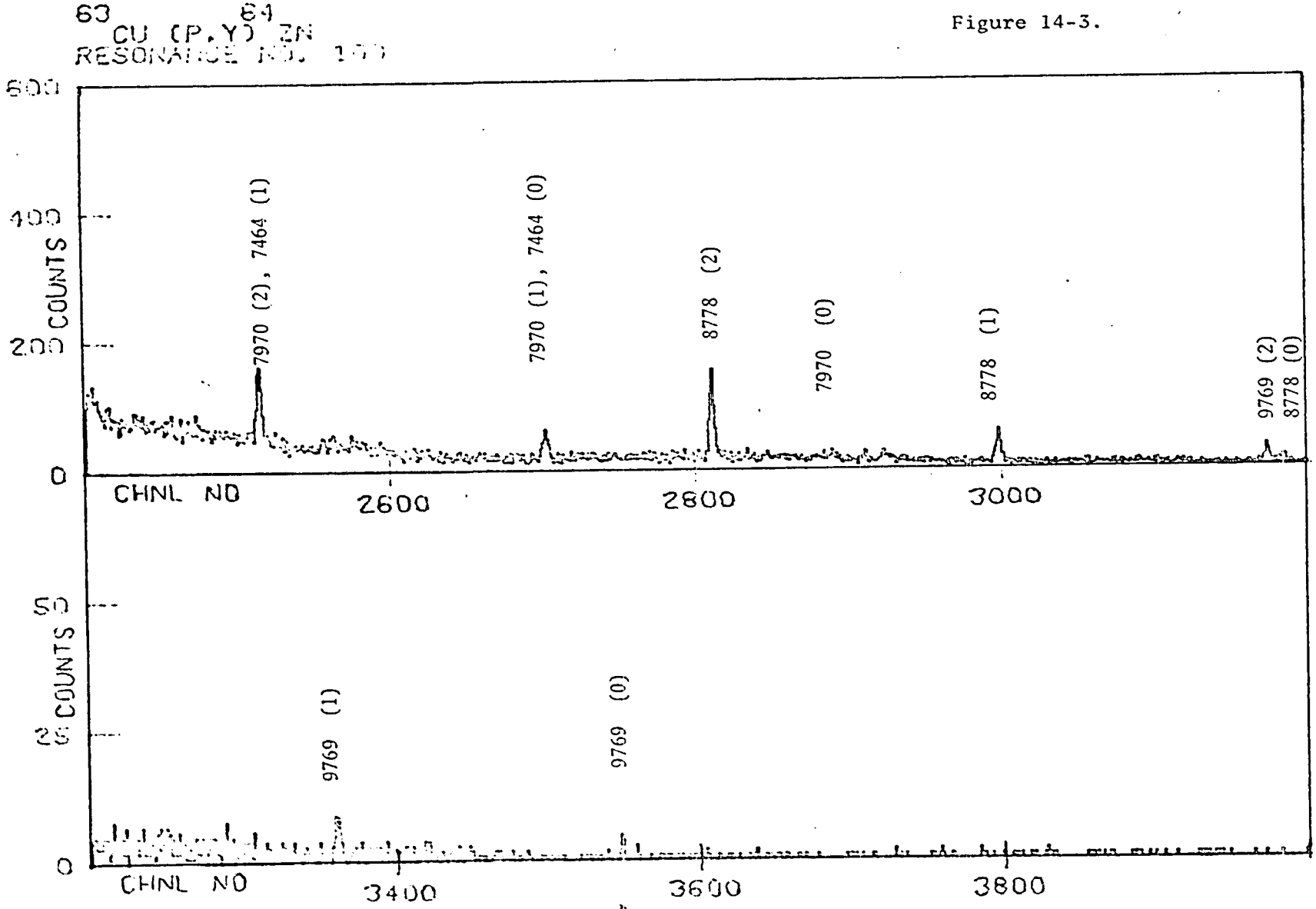
63 64
CU (P,Y) ZN
RESONANCE NO. 177
600
400
200
0
COUNTS
7970 (2), 7464 (1)
7970 (1), 7464 (0)
8778 (2)
7970 (0)
8778 (1)
9769 (2)
8778 (0)
CHNL NO
2600
2800
3000
50
25
0
COUNTS
9769 (1)
9769 (0)
CHNL NO
3400
3600
3800

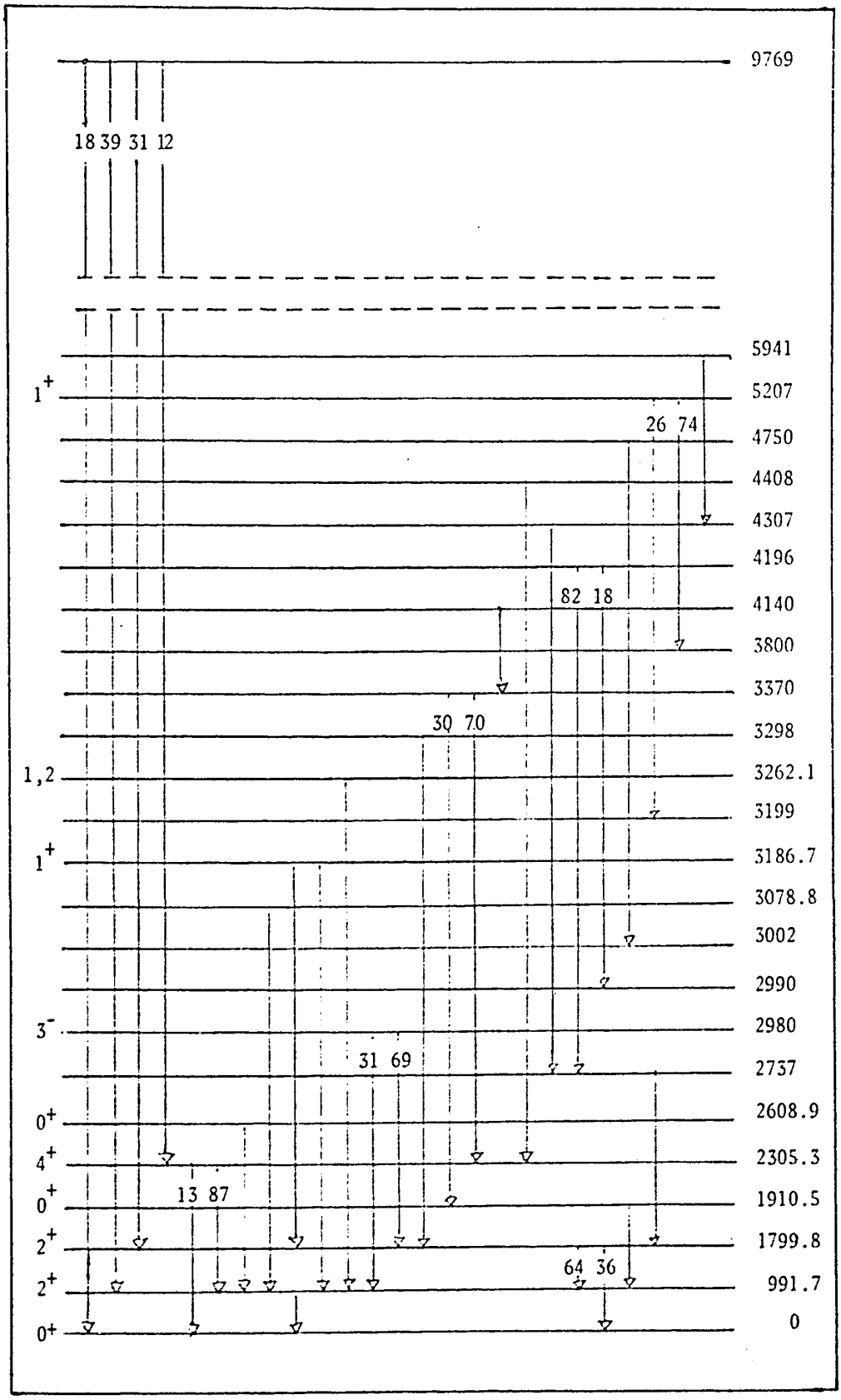

Figure 15 Decay Scheme of ^{64}Zn from resonance no. 100

Tables 3-1, 3-2, and 3-3 show energies, branching ratio, and assingments of γ-rays which were observed at resonance no. 100, 94, and 69 and comparisons with $^{64}Ga(\beta^{+})^{64}Zn$ decay and $^{64}Zn(p, p'\gamma)^{64}Zn$ reaction " Energies in Kev's"

Initial State	Present Work				$^{64}Ga(\beta^{+})^{64}Zn$ Decay			$^{64}Zn(p\ p'\gamma)^{64}Zn$	
	Final State	Resonance number	Gamma-ray	Branching ratio (%)	Final State	gamma-ray	Branching ratio	Final State	gamma-ray
9769	0	100	9769 ± 2	18					
	991.7	100	8778 ± 1	39					
	1799.8	100	7970 ± 1	31					
	2305.3	100	7464 ± 1	12					
9732	0	94	9732 ± 2	3					
	991.7	94	8741 ± 1	65					
	1799.8	94	7934 ± 1	15					
	2305.3	94	7427 ± 1	3					
	2789	94	6943 ± 1	14					
9600	0	69	9600 ± 1	16					
	991.7	69	8609 ± 1	20					
	1799.8	69	7800 ± 1	57					

Table 3-2

Initial State	Present Work				$^{64}Ga(\beta^+)^{64}Zn$ Decay			$^{64}Zn(p\ p'\gamma)^{64}Zn$	
	Final State	Resonance number	Gamma-ray	Branching ratio (%)	Final State	gamma-ray	Branching ratio	Final State	gamma-ray
9600	2305.3	69	7295 ± 1	7					
5941	4307	100, 94, 69	1633 ± 0.5						
5207	3199	100, 94, 69	2007 ± 0.5	26	991.6	4215	0.1		
	3800	100, 94, 69	1406.7±0.5	74					
4750	3002	100	1747.6±0.5		0	4749	0.05		
4408	2305.3	100, 94, 69	2102.7±0.5						
4307	2737	100, 94, 69	1570.4±0.5						
4196	2737	100, 94, 69	(1460.8±0.5)	82					
	2990	100, 94, 69	1206.2±0.5	18					
4140	5370	100	7704 ± 0.5					0	4140
3370	1799.8	100, 94, 69	1570.4±0.5	30				0	3370
	1910.5	100, 94, 69	1460.4±0.5	70				1902	1430
3298	1910.5	100 94, 69	1387.8±0.5						
3262.1	991.7	100, 94, 69	2270.2±0.5		991.6	2270.5	2.3		
					0	3262.9	0.3		

Table 3-3.

Initial State	Present Work				$^{64}Ga(\beta^+)^{64}Zn$ Decay			$^{64}Zn(p\ p'\gamma)^{64}Zn$	
	Final State	Resonance number	Gamma-ray	Branching ratio (%)	Final State	gamma-ray	Branching ratio	Final State	gamma-ray
3186	991.7	$^{100,94,}_{69}$	2195.6±0.5		991.6	2195.2	11		
	1799.8	$^{100,94,}_{69}$	1386.5±0.5		1799.7	1386.9	14		
					1910.5	1276.4	6.9		
3078.8	991.7	$^{100,94,}_{69}$	2087.1±0.5						
2980	991.7	$^{100,94,}_{69}$	1987.6±0.5	31					
	1799.8	$^{100,94,}_{69}$	1180.4±0.5	69					
2737	1799.8	$^{100,94,}_{69}$	936.7± 0.5						
2608.9	991.7	$^{100,94,}_{69}$	1618.3±0.5		991.6	1617.2	1.7	991.3	1623
2305.3	0	$^{100,94,}_{69}$	2305.3±0.5	13					
	991.7	$^{100,94,}_{69}$	1314.8	87				991.3	1329
1910.5	991.7	$^{100,94,}_{69}$	918.8±0.5		991.6	918.9	8.3	991.3	911
1799.8	0	$^{100,94,}_{69}$	1799.8±0.5	36	0	1799.3	4.6	0	1804 (24%)
	991.7	$^{100,94,}_{69}$	808.1±0.5	64	991.6	808.8	1.4	991.3	810 (76%)
991.7	0	$^{100,94,}_{69}$	991.2±0.5	100	0	991.6	46	0	994

CHAPTER VII DISCUSSION

The figures 5-1, 5-2, 5-3 and Figure 7 show that the level density of the medium weight elements at high exciation energy is quite high. From Figure 6 it appears that the valleys of the peaks are very large compared with the general background. It seems that the target of 3 Kev thickness and 1 Kev steps was not good enough for taking the excitation curve. It might be necessary to use a target of 1 Kev thickness and 0.5 Kev steps for taking the excitation curve of the medium weight elements in the (p, γ) reaction because the Q-value in this reaction is higher than in others. But it is very difficult to get good statistics with a target of 1 Kev thickness because the yield is too small. It is more difficult to use 0.5 Kev steps to take the excitation curve without an analysing magnet being available because the beam energy spread is 1 - 2 Kev at incident proton energy up to 2 Mev.

Theoretical calculations for the nuclear level density ^{64}Zn are very rough compared with the experimental result. The best one is Bethe's theory using Gilbert and Cameron's correction of the excitation energy and parameter a.

The best agreement of our experimental results with theoretical calculations occured with the analogue states. This is because accurate values for the coulomb displacement energy were available at the time of writing. Unfortunately, the spins and parities of the low energy levels of ^{64}Cu are still not well known. From the results, the analogue states appear to be 1^+ for 9.400 Mev, $?^+$ for 0.554 Mev and 2^+ for 9.598 Mev in ^{64}Zn. These values can only be verified by an angular distribution experiment.

The most successful aspect of the present work was the energy calibration of gamma-rays taken by the Ge(Li) detector. Unfortunately, the beam energy spread and shift caused a high background below 5 Mev which tended to obscure the weak γ-ray transitions in that region. If the analysing magnet and a shielded area for the target had been available, the work on the (p, γ) reaction in medium weigh weight elements would have met with even better success.

REFERENCES

(1) C. W. Malich and J. C. Harns, Phys. Rev. 81 (1951) 318

(2) C. E. Weller and J. C. Grosskreutz. Phys. Rev. 102 (1956) 1149.

(3) H. A. Bethe. Rev. Mod. Phys. 9 (1937) 69

(4) C. Van Lier and G. E. Uhlenbeck. physica 4 (1937) 531

(5) J. M. B. Lang and K. J. LeCouteur. Proc. Phys. Soc. London A64 (1954) 585.

(6) T. D. Newton. Can. J. Phys. 34 (1958) 804

(7) A. G. W. Cameron. Can. J. Phys. 36 (1958) 1040

(8) T. Ericson. Advan. Phys. 9 (1960) 425

(9) A. Gilbert and A. G. W. Cameron. Can. J. Phys. 43 (1965) 1446

(10) M. G. Mayer and J. H. D. Jensen. Elementary Theory of Nuclear Shell Structure. (John Wiley & Sons, New York, 1955)

(11) J. D. Anderson and C. Wong. Phys. Rev. Lett 7 (1961) 250

(12) J. D. Anderson, C. Wong and J. W. McClure.
Phys. Rev. 126 (1962) 2170

(13) J. D. Anderson, C. Wong and J. W. McClure.
Phys. Rev. 129 (1963) 2718

(14) A. M. Lane. Phys. Rev. Lett 8 (1962) 171

(15) A. M. Lane. Nucl. Phys. 35 (1962) 676

(16) N. V. J. Swamy and A. E. S. Green
Phys. Rev. 112 (1958) 1719

(17) Y. P. Antonfiev. Nucl. Phys. 46 (1963) 1

(18) M. A. Meyer, N. S. Wolmaraus and D. Reitmann
Nucl. Phys. A 144 (1970) 261

(19) Mattach Nucl. Phys. 67 (1965) 73

(20) M. Harchol etc. Nucl. Phys. 79 (1966) 165

(21) R. L. Auble, W. C. McHarris, W. H. Kelly
Bull. Am. Phys. Soc. 12, No. 1, 128, HF 3 (1967)

(22) J. Konijn, R. van Lieshout, J. P. Deutsch,
L. Grenacs. Nucl. Phys. A91, 439 (1967).

(23) L. G. Mann, K. G. Tirsell, S. D. Bloom
Nucl. Phys. A97, 425 (1967)

(24) D. M. Van Patter, S. M. Shafroth, P. F. Hinnchsen
Bull. Am. Phys. Soc. 11, No. 3 407, KA11 (1966)

APPENDIX

Figure 16

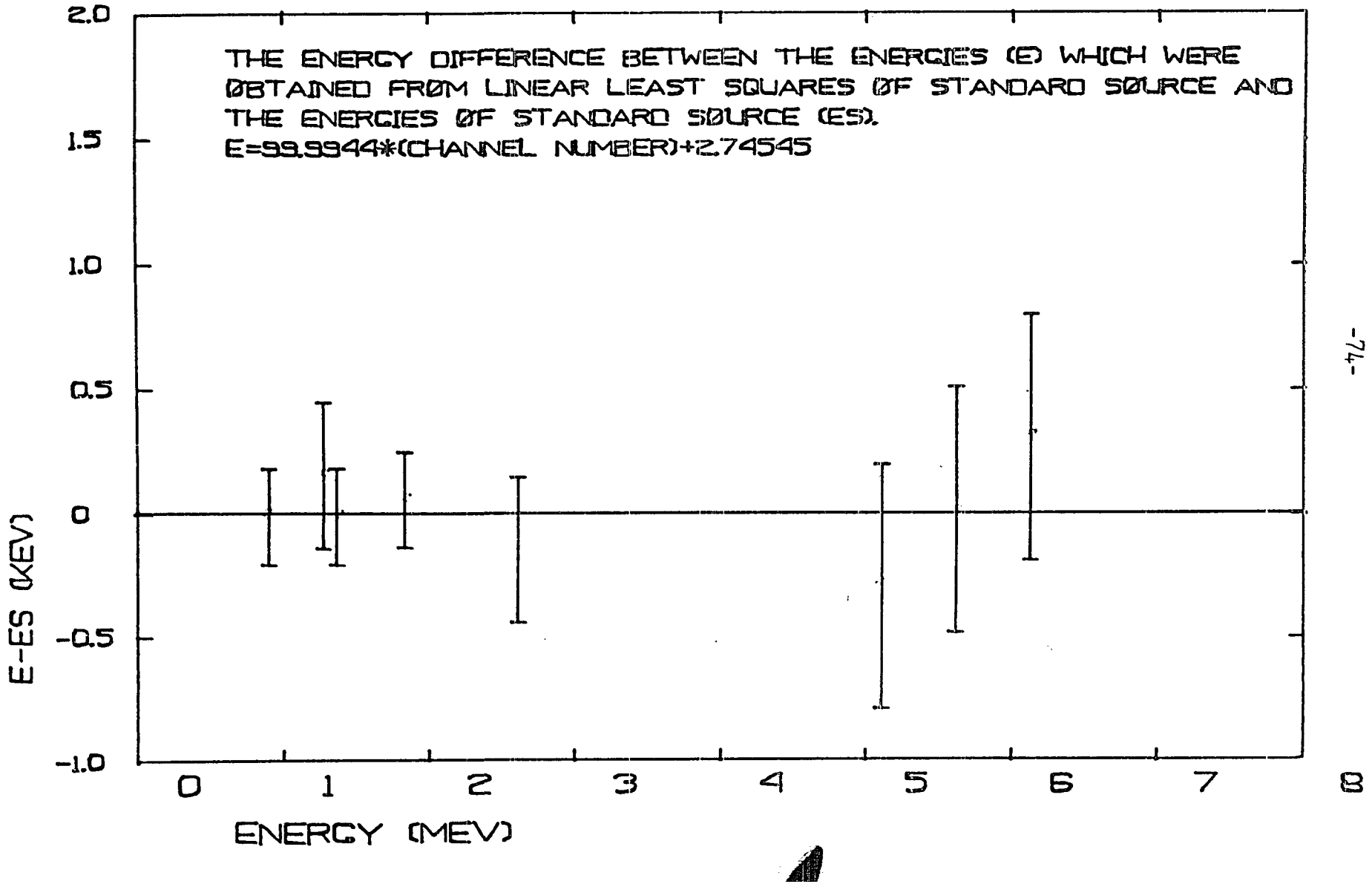
THE ENERGY DIFFERENCE BETWEEN THE ENERGIES (E) WHICH WERE
OBTAINED FROM LINEAR LEAST SQUARES OF STANDARD SOURCE AND
THE ENERGIES OF STANDARD SOURCE (ES).
E=99.9944*(CHANNEL NUMBER)+2.74545
2.0
1.5
1.0
0.5
0
-0.5
-1.0
E-ES (KEV)
0
1
2
3
4
5
6
7
8
ENERGY (MEV)

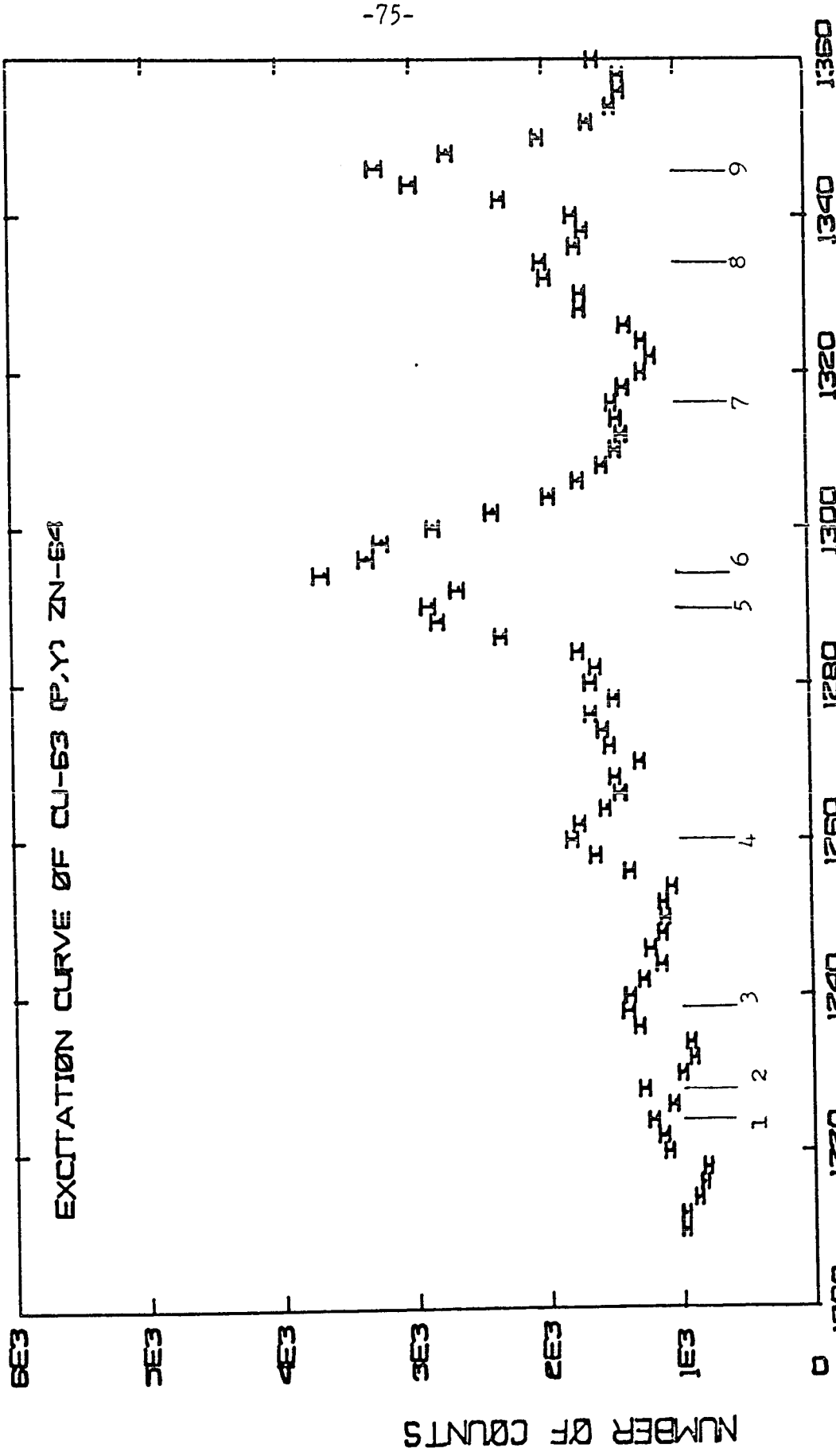
EXCITATION CURVE OF CU-63 (P,Y) ZN-63
NUMBER OF COUNTS
DIGITAL VOLTMETER READING
0
1E3
2E3
3E3
4E3
5E3
1200
1220
1240
1260
1280
1300
1320
1340
1360
1
2
3
4
5
6
7
8
9

Figure 17-1

Figure 17-2

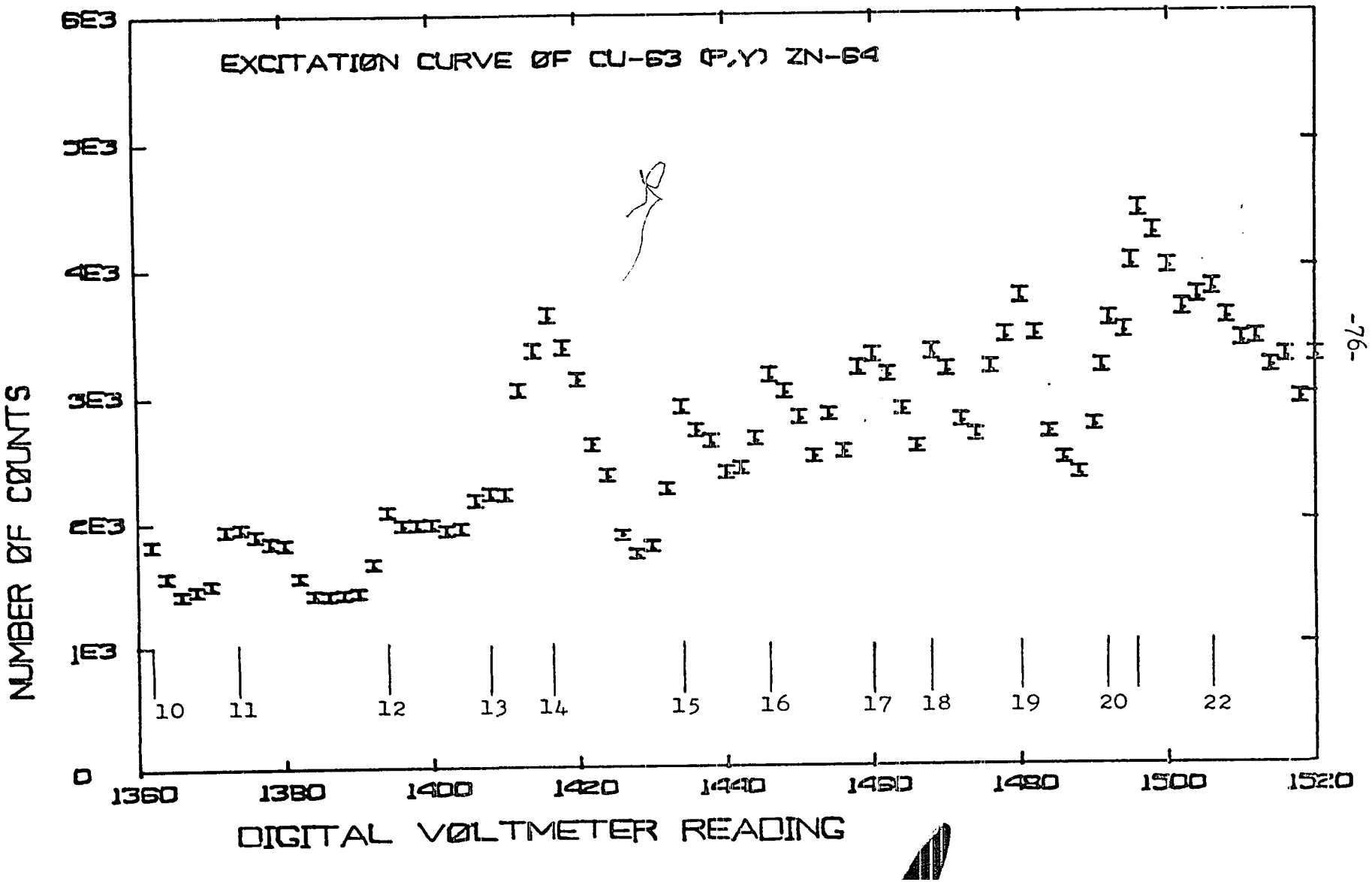
EXCITATIØN CURVE ØF CU-63 (P,Y) ZN-64
NUMBER ØF CØUNTS
6E3
5E3
4E3
3E3
2E3
1E3
0
10
11
12
13
14
15
16
17
18
19
20
22
1360
1380
1400
1420
1440
1460
1480
1500
1520
DIGITAL VØLTMETER READING

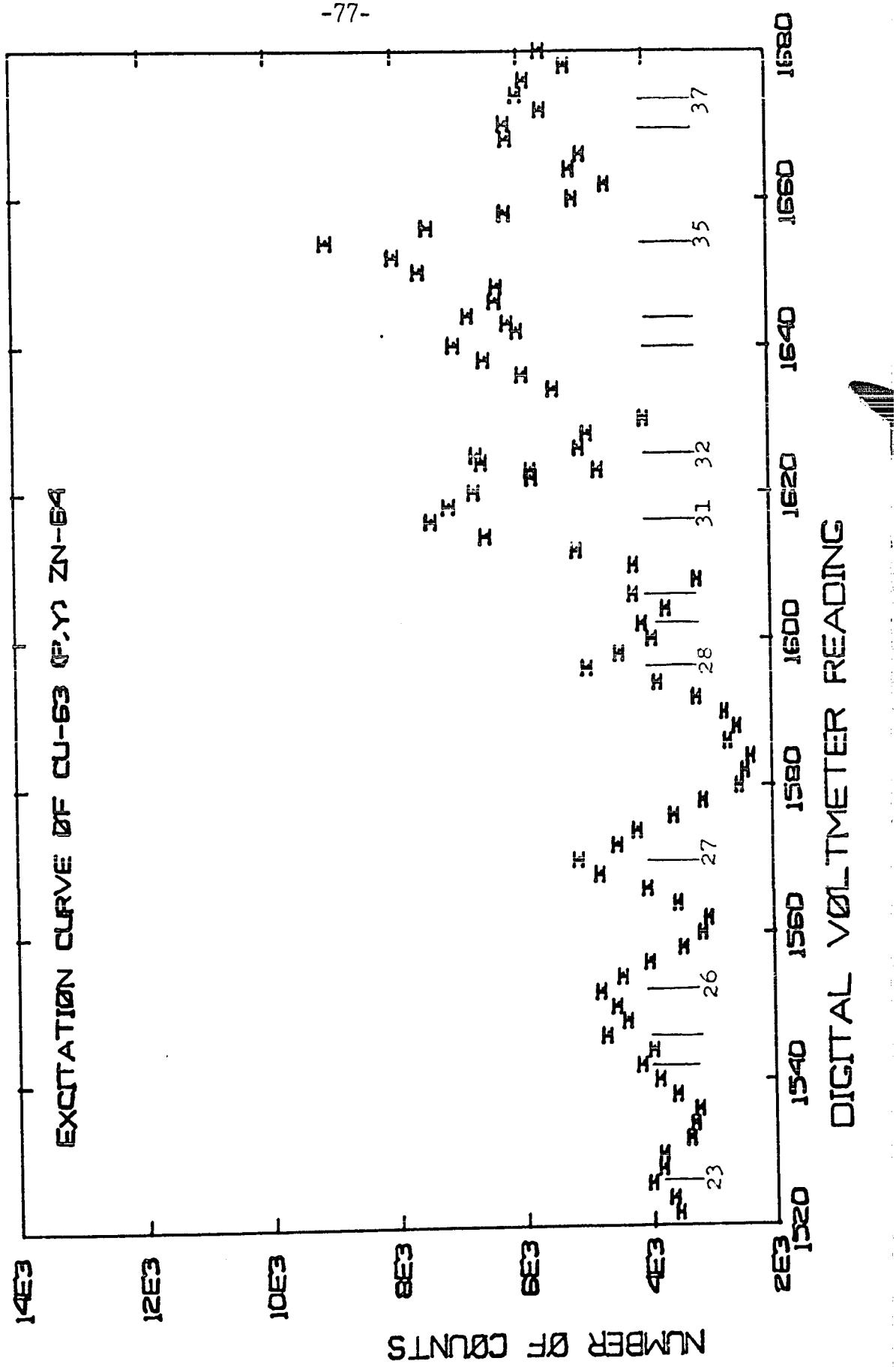
EXCITATION CURVE OF CU-63 (P,Y) ZN-64
NUMBER OF COUNTS
DIGITAL VOLTMETER READING
14E3
12E3
10E3
8E3
6E3
4E3
2E3
1520
1540
1560
1580
1600
1620
1640
1660
1680
23
26
27
28
31
32
35
37

Figure 17-3

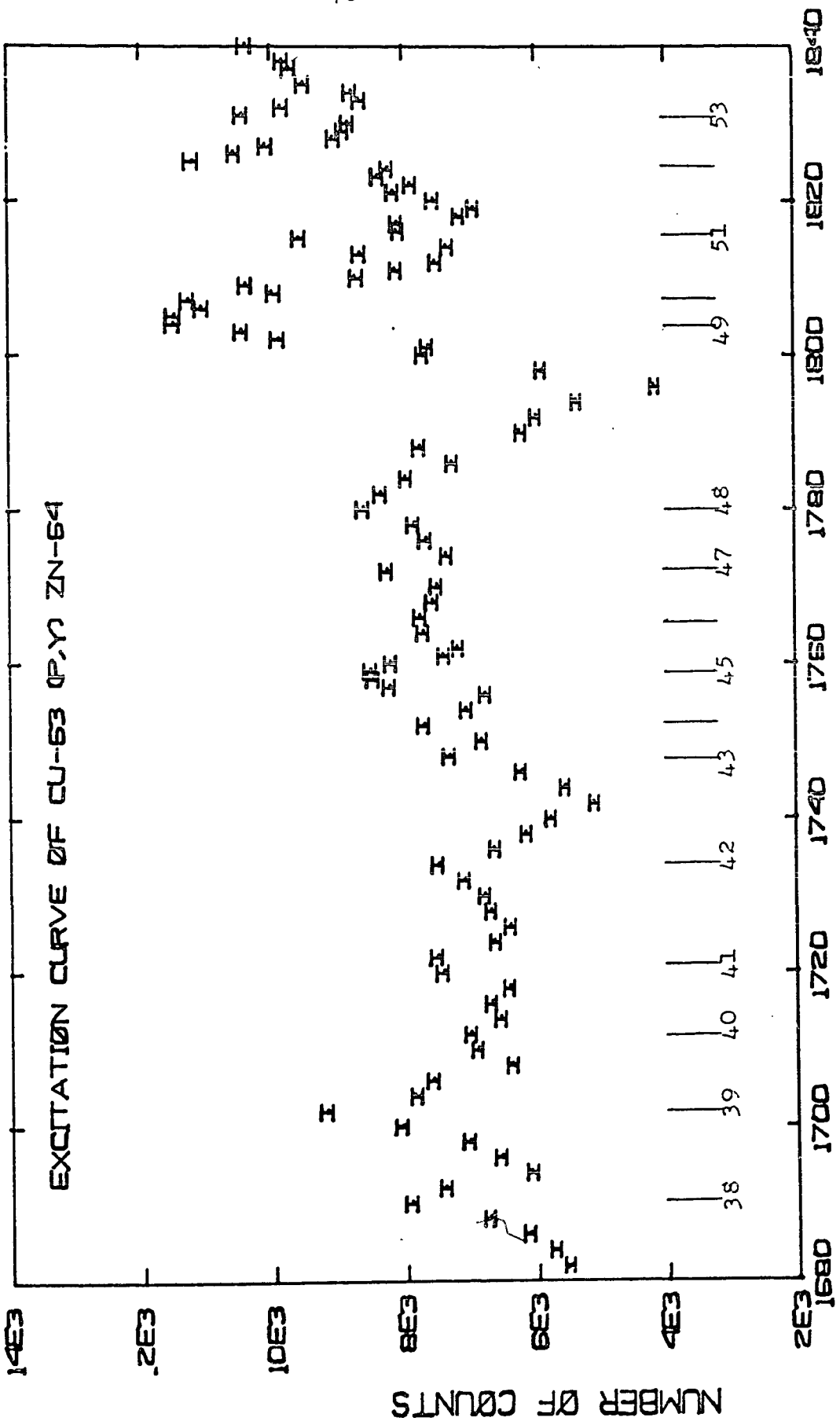
EXCITATION CURVE OF CU-63 (P,Y) ZN-64
NUMBER OF COUNTS
DIGITAL VOLTMETER READING
1E3
2E3
4E3
6E3
8E3
10E3
14E3
1680
1700
1720
1740
1760
1780
1800
1820
1840
38
39
40
41
42
43
45
47
48
49
51
53

Figure 17-4

Figure 17-5

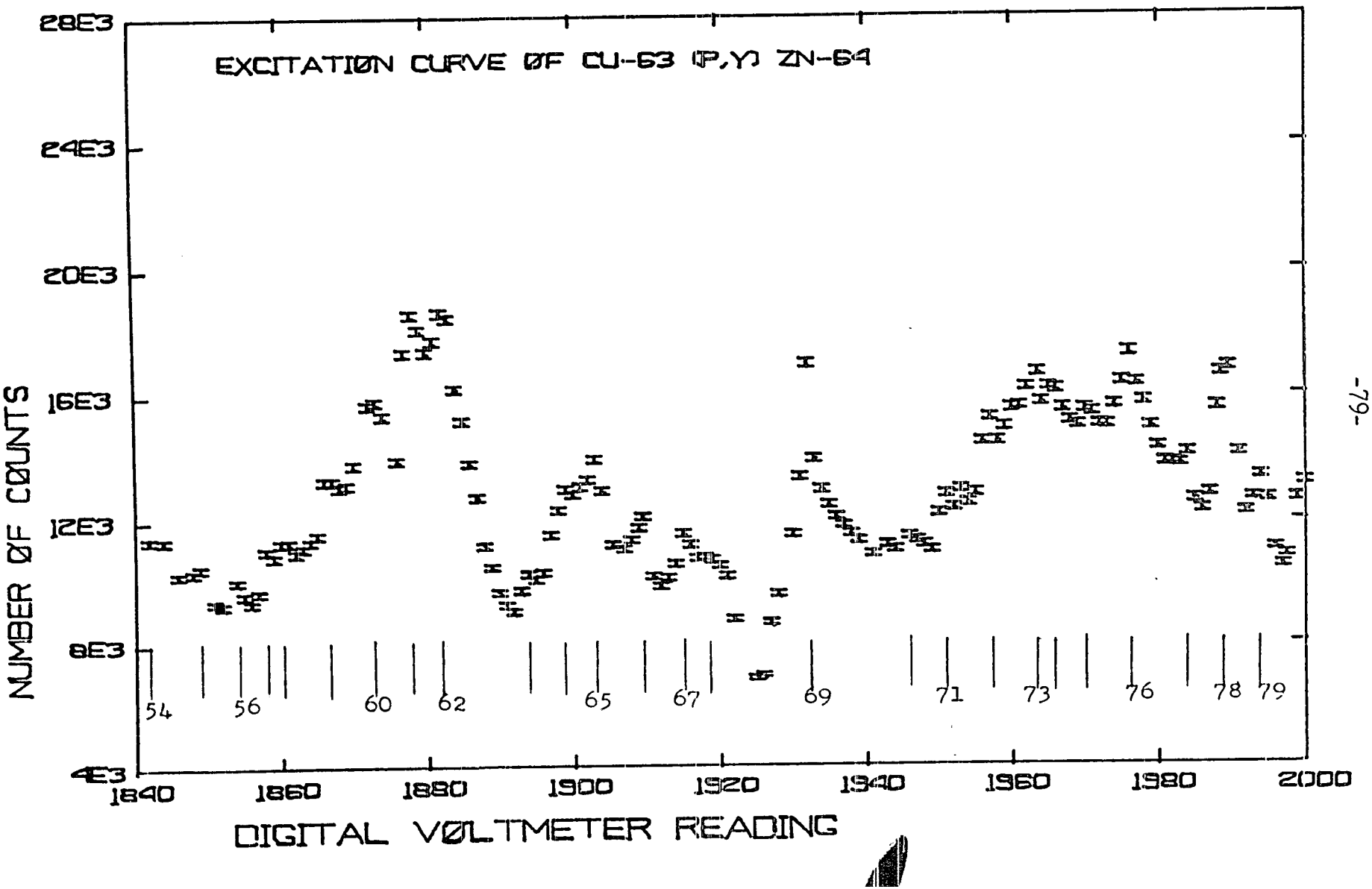
EXCITATION CURVE OF CU-63 (P,Y) ZN-64
NUMBER OF COUNTS
28E3
24E3
20E3
16E3
12E3
8E3
4E3
1840
1860
1880
1900
1920
1940
1960
1980
2000
DIGITAL VOLTMETER READING
54
56
60
62
65
67
69
71
73
76
78
79

Figure 17-6

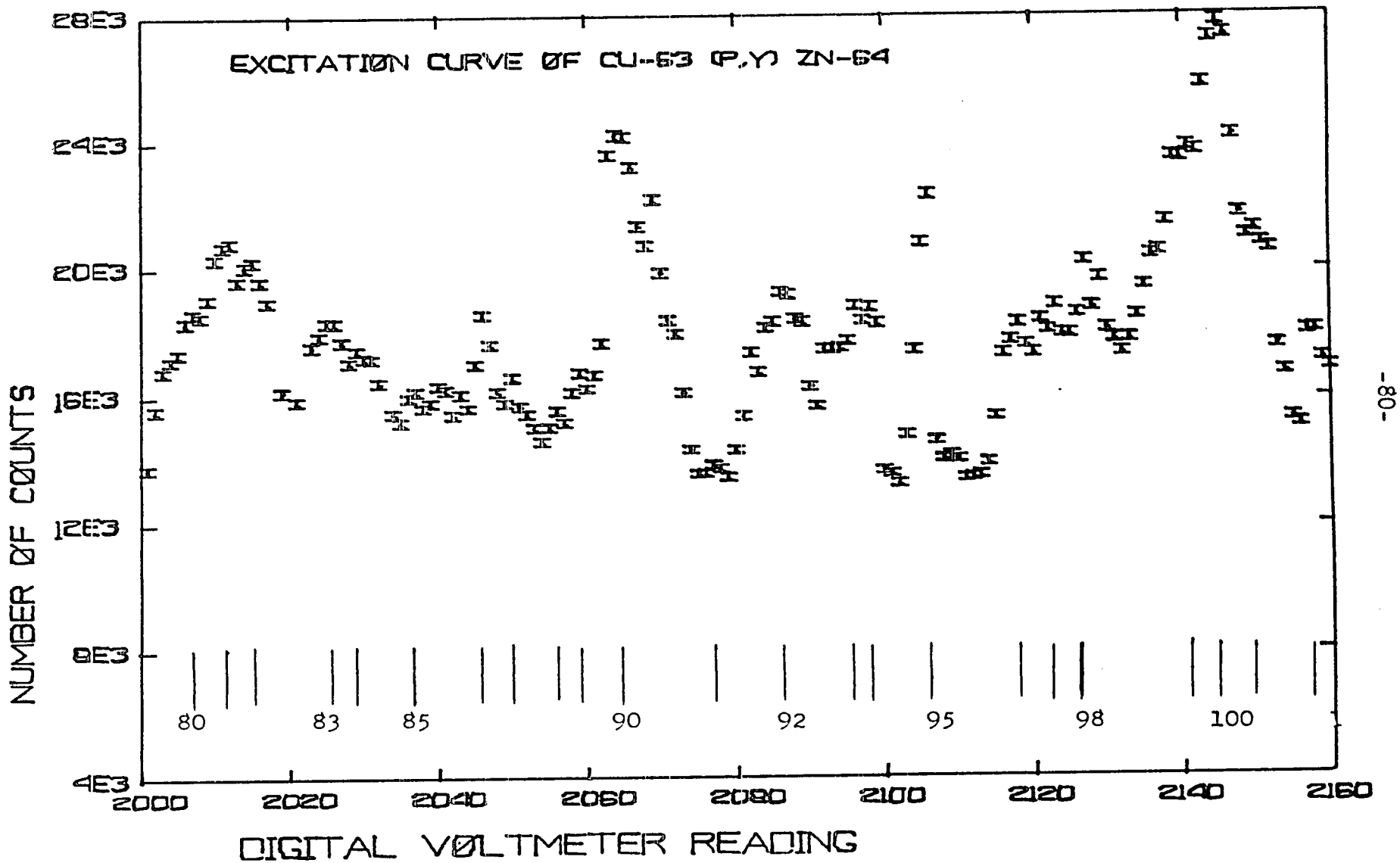
EXCITATION CURVE OF CU-63 (P,Y) ZN-64
NUMBER OF COUNTS
28E3
24E3
20E3
16E3
12E3
8E3
4E3
2000
2020
2040
2060
2080
2100
2120
2140
2160
80
83
85
90
92
95
98
100
DIGITAL VOLTMETER READING

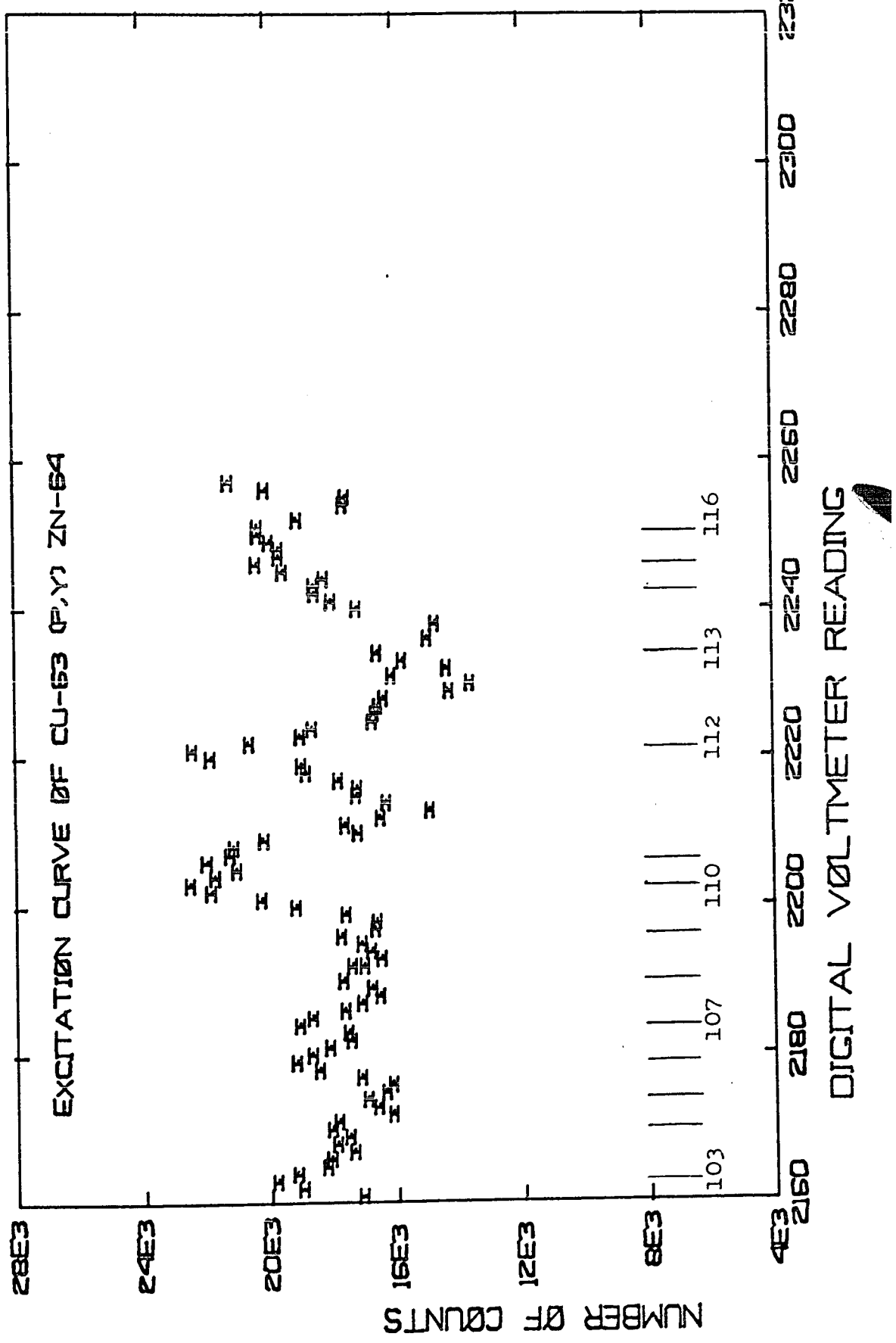
EXCITATION CURVE OF CU-63 (P,Y) ZN-64
NUMBER OF COUNTS
28E3
24E3
20E3
16E3
12E3
8E3
4E3
2160
2180
2200
2220
2240
2260
2280
2300
2320
DIGITAL VOLTMETER READING
103
107
110
112
113
116

Figure 17-7